

# Physics and applications of atmospheric nonlinear optics and filamentation

Jérôme Kasparian<sup>1,2\*</sup>, Jean-Pierre Wolf<sup>1</sup>

<sup>1</sup>GAP, Université de Genève, 20 rue de l'École de Médecine, CH-1211 Genève, Switzerland

<sup>2</sup>LASIM (UMR5579), Université Claude Bernard Lyon 1, 43 bd du 11 Novembre, F-69622 Villeurbanne Cedex, France.

\* Corresponding author: [jkaspari@lasim.univ-lyon1.fr](mailto:jkaspari@lasim.univ-lyon1.fr)

**Abstract:** We review the properties and applications of ultrashort laser pulses in the atmosphere, with a particular focus on filamentation. Filamentation is a non-linear propagation regime specific of ultrashort and ultraintense laser pulses in the atmosphere. Typical applications include remote sensing of atmospheric gases and aerosols, lightning control, laser-induced spectroscopy, coherent anti-stokes Raman scattering, and the generation of sub-THz radiation.

©2008 Optical Society of America

**OCIS codes:** (190.7110) Ultrafast non-linear optics; (140.7090) Ultrafast lasers; (190.3270) Kerr effect; (190.5530) Pulse propagation and solitons; (260.5950) Self-focusing; (190.5940) Self-action effects; (120.0280) Remote sensing; (280.3640) Lidar; (290.1090) Aerosol and cloud effects; (280.1310) Atmospheric scattering; (290.1350) Backscattering; (350.5400) Plasmas; (999.9999) Lightning control; (190.4180) Multiphoton processes; (010.7060) Turbulence; (010.3310) Laser beam transmission;

---

## References and Links

1. P. L. Kelley, "Self-focusing of optical beams," *Phys. Rev. Lett.* **15**, 1005-1008 (1965); Erratum in *Phys. Rev. Lett.* **16**, 384 (1965)
2. G. A. Askar'yan, "The self-focusing effect," *Sov. Phys. J.* **16** 680 (1974)
3. A. Braun, G. Korn, X. Liu, D. Du, J. Squier, G. Mourou, "Self-channeling of high-peak-power femtosecond laser pulses in air," *Opt. Lett.* **20**, 73-75 (1995)
4. L. Roso-Franco, "Self-reflected wave inside a very dense saturable absorber," *Phys. Rev. Lett.* **55**, 2149-2151 (1985)
5. R. R. Alfano, S. L. Shapiro, "Emission in the region 4000 to 7000 Å," *Phys. Rev. Lett.* **24**, 584-587 (1970)
6. R. R. Alfano, S. L. Shapiro, "Observation of self-phase modulation and small-scale filaments in crystals and glasses," *Phys. Rev. Lett.* **24**, 592-595 (1970)
7. R. R. Alfano, S. L. Shapiro, "Direct distortion of electric clouds of rare-gas atoms in intense electric fields," *Phys. Rev. Lett.* **24**, 1217-1220 (1970)
8. A. Brodeur, S. L. Chin, "Ultrafast white-light continuum generation and self-focusing in transparent condensed media," *J. Opt. Soc. Am. B* **16**, 637-650 (1999)
9. Y. Shen, "The principles of nonlinear optics," John Wiley & Sons (1984)
10. G. Yang, Y. Shen, "Spectral broadening of ultrashort pulses in a nonlinear medium," *Opt. Lett.* **9**, 510-512 (1984)
11. A. L. Gaeta, "Catastrophic collapse of ultrashort pulses," *Phys. Rev. Lett.* **84**, 3582-3585 (2000)
12. K. Ranka, R. W. Schirmer, A. L. Gaeta, "Observation of pulse splitting in nonlinear dispersive media," *Phys. Rev. Lett.* **77**, 3783-3786 (1996)
13. A. Proulx, A. Talebpour, S. Petit, S. L. Chin, "Fast pulsed electric field created from the self-generated filament of a femtosecond Ti:Sapphire laser pulse in air," *Opt. Commun.* **174**, 305-309 (2000)
14. S. Tzortzakis, M. A. Franco, Y.-B. André, A. Chiron, B. Lamouroux, B. S. Prade, A. Mysyrowicz, "Formation of a conducting channel in air by self-guided femtosecond laser pulses," *Phys. Rev. E* **60**, R3505-R3507 (1999)
15. S. Tzortzakis, B. Prade, M. Franco, A. Mysyrowicz, "Time evolution of the plasma channel at the trail of a self-guided IR femtosecond laser pulse in air," *Optics Commun.* **181**, 123-127 (2000)
16. H. Schillinger, R. Sauerbrey, "Electrical conductivity of long plasma channels in air generated by self-guided femtosecond laser pulses," *Appl. Phys. B* **68**, 753-756 (1999)
17. D. Strickland, G. Mourou, "Compression of amplified chirped optical pulses," *Opt. Commun.* **56**, 219-221 (1985)

18. P. Maine, D. Strickland, P. Bado, M. Pessot, G. Mourou, "Generation of ultrahigh peak power pulses by chirped pulse amplification," *IEEE J. Quantum Electron.* **24**, 398-403 (1988)
19. D. Faccio, A. Averchi, A. Couairon, M. Kolesik, J. V. Moloney, A. Dubietis, G. Tamosauskas, P. Polesana, A. Piskarskas, and P. Di Trapani, "Spatio-temporal reshaping and X Wave dynamics in optical filaments," *Opt. Express* **15**, 13077-13095 (2007)
20. H. J. Kölsch, P. Rairoux, J.-P. Wolf, L. Wöste, "Comparative study of nitric-oxide immission in the cities of Lyon, Geneva and Stuttgart using a mobile differential absorption Lidar system," *Appl. Phys. B* **54**, 89-94 (1992)
21. H. J. Kölsch, P. Rairoux, J.-P. Wolf, L. Wöste, "Simultaneous NO and NO<sub>2</sub> measurement using BBO crystals," *Appl. Opt.* **28**, 2052-2056 (1989)
22. J.P. Wolf, UV-DIAL-Lidar Techniques for Air Pollution Monitoring, in "Encyclopedia of Analytical Chemistry," Ed. R.A. Meyers, Vol 3, pp 2226-2247, J. Wiley & Sons, New York (2000)
23. E. Fréjafon, J. Kasparian, P. Rambaldi, B. Vezin, V. Boutou, J. Yu, M. Ulbricht, D. Weidauer, B. Ottobriani, E. de Saeger, B. Krämer, T. Leisner, P. Rairoux, L. Wöste, and J.P. Wolf, "Laser applications for atmospheric pollution monitoring," *European Physical Journal D*, **4**, 231-238 (1998)
24. P. Rambaldi, M. Douard, J.-P. Wolf, "New UV tunable solid-state lasers for Lidar applications," *Appl. Phys. B* **61**, 117-120 (1995)
25. O. Duclaux, E. Fréjafon, H. Schmidt, A. Thomasson, D. Mondelain, J. Yu, C. Guillaumond, C. Puel, F. Savoie, P. Ritter, J. P. Boch, J. P. Wolf, "3D-air quality model evaluation using the Lidar technique," *Atmos. Environ.* **36**, 5081-5095 (2002)
26. M. Beniston, J.-P. Wolf, M. Beniston-Rebetez, H. J. Kölsch, P. Rairoux, L. Wöste, "Use of Lidar Measurements and numerical models in air-pollution research," *J. Geophys. Res. - Atmospheres* **95** (D7), 9879-9894 (1990)
27. H.L. Walmsley, S.J. O'Connor, "The accuracy and sensitivity of infrared differential absorption lidar measurements of hydrocarbon emissions from process units," *Pure and Appl. Opt.* **7**, 907-925 (1998)
28. M. Douard, R. Bacis, G. Fabre, P. Rambaldi, A. Ross, R. Stringat, J.P. Wolf, "Fourier-Transform Lidar," *Opt. Lett.* **20**, 2140-2142 (1995)
29. F.A. Theopold, A. Behrendt, H. Flint, C. Weitkamp, Dial revisited: Belinda and white-light femtosecond Lidar, in "Advances in Atmospheric Remote Sensing with Lidar," Springer-Verlag, Berlin, (1996) 590 pp. p.325-328.
30. M. del Guasta, M. Morandi, L. Stefanutti, B. Stein, J. Kolenda, P. Rairoux, J.P. Wolf, R. Matthey, E. Kyrö, "Multiwavelength lidar observation of thin cirrus at the base of the Pinatubo stratospheric layer during the EASOE campaign," *Geophys. Res. Lett.*, **21**, 1339-1342 (1994);
31. M. del Guasta, M. Morandi, L. Stefanutti, B. Stein, J.P. Wolf, "Derivation of mount Pinatubo stratospheric aerosol mean size distribution by means of a multiwavelength Lidar," *App. Optics* **33**, 5690-5697 (1994)
32. B. Stein, M. Delgusta, J. Kolenda, M. Morandi, P. Rairoux, L. Stefanutti, J.-P. Wolf, L. Wöste, "Stratospheric aerosol-size distributions from multispectral Lidar measurements at Sodankyla during EASOE," *Geophys. Res. Lett.* **21**, 1311-1314 (1994)
33. J. Kasparian, E. Fréjafon, P. Rambaldi, J. Yu, P. Ritter, P. Viscardi, J.P. Wolf, "Characterization of urban aerosols using SEM-microscopy, X-Ray analysis, and Lidar measurements," *Atmospheric Environment* **32**, 2957-2967 (1998)
34. L. Wöste, C. Wedekind, H. Wille, P. Rairoux, B. Stein, S. Nikolov, C. Werner, S. Niedermeier, F. Ronneberger, H. Schillinger, R. Sauerbrey, "Femtosecond atmospheric lamp," *Laser und Optoelektronik*, **E 2688**, (1997)
35. P. Rairoux, H. Schillinger, S. Niedermeier, M. Rodriguez, F. Ronneberger, R. Sauerbrey, B. Stein, D. Waite, C. Wedekind, H. Wille, L. Wöste, C. Ziener, "Remote sensing of the atmosphere using ultrashort laser pulses," *App. Phys. B* **71**, 573-580 (2000)
36. S. L. Chin, S.A. Hosseini, W. Liu, Q. Luo, F. Theberge, N. Aközbek, A. Becker, V. P. Kandidov, O. G. Kosareva, H. Schroeder, "The propagation of powerful femtosecond laser pulses in optical media: physics, applications, and new challenges," *Can. J. Phys.* **83**, 863-905 (2005)
37. Couairon, A. Mysyrowicz, "Femtosecond filamentation in transparent media," *Physics Reports* **441**, 47-189 (2007)
38. L. Bergé, S. Skupin, R. Nuter, J. Kasparian, J.-P. Wolf, "Ultrashort filaments of light in weakly-ionized, optically-transparent media," *Rep. Prog. Phys.* **70**, 1633-1713 (2007)
39. H. Wille, M. Rodriguez, J. Kasparian, D. Mondelain, J. Yu, A. Mysyrowicz, R. Sauerbrey, J.-P. Wolf, and L. Wöste, "Teramobile: a mobile femtosecond-terawatt laser and detection system," *European Physical Journal - Appl. Phys.* **20**, 183-190 (2002)
40. A. Talebpour, J. Yang, S.L. Chin, "Semi-empirical model for the rate of tunnel ionization of N<sub>2</sub> and O<sub>2</sub> molecules in an intense Ti:sapphire laser pulse," *Optics Commun.* **163**, 29-32 (1999)
41. L.V. Keldysh, "Ionization in field of a strong electromagnetic wave," *Sov. Phys. JETP* **20**, 1307 (1965)
42. L. Bergé, A. Couairon, "Gas-induced solitons," *Phys. Rev. Lett.* **86**, 1003-1006 (2001)
43. A. Becker, N. Aközbek, K. Vijayalakshmi, E. Oral, C.M. Bowden, and S.L. Chin, "Intensity clamping and re-focusing of intense femtosecond laser pulses in nitrogen molecular gas," *Appl. Phys. B*, **73**, 287-290 (2001)
44. J. Kasparian, R. Sauerbrey, S.L. Chin, "The critical laser intensity of self-guided light filaments in air," *Appl. Phys. B*, **71**, 877-879 (2000)
45. W. G. Wagner, H. A. Haus, J. H. Marburger, "Large-scale self-trapping of optical beams in the paraxial ray approximation," *Phys. Rev.* **175**, 256-266 (1968); Erratum in *Phys. Rev. A*, **3**, 2150 (1971)

46. G. Méjean, J. Kasparian, J. Yu, E. Salmon, S. Frey, J.-P. Wolf, S. Skupin, A. Vinçotte, R. Nuter, S. Champeaux, and L. Bergé, "Multifilamentation transmission through fog," *Phys. Rev. E* **72**, 026611 (2005)
47. P. Béjot, L. Bonacina, J. Extermann, M. Moret, J.P. Wolf, R. Ackermann, N. Lascoux, R. Salamé, E. Salmon, J. Kasparian, L. Bergé, S. Champeaux, C. Guet, N. Blanchot, O. Bonville, A. Boscheron, P. Canal, M. Castaldi, O. Hartmann, C. Lepage, L. Marmande, E. Mazataud, G. Mennerat, L. Patisou, V. Prevot, D. Raffestin, J. Ribolzi, "32 Terawatt Atmospheric White-Light Laser," *Appl. Phys. Lett.* **90**, 151106 (2007)
48. B. La Fontaine, F. Vidal, Z. Jiang, C.Y. Chien, D. Comtois, A. Desparois, T.W. Johnson, J.-C. Kieffer, and H. Pépin, "Filamentation of ultrashort pulse laser beams resulting from their propagation over long distances in air," *Physics of plasmas* **6**, 1615-1621 (1999)
49. M. Rodriguez, R. Bourayou, G. Méjean, J. Kasparian, J. Yu, E. Salmon, A. Scholz, B. Stecklum, J. Eislöffel, U. Laux, A.P. Hatzes, R. Sauerbrey, L. Wöste, and J.-P. Wolf, "Kilometer-range non-linear propagation of femtosecond laser pulses," *Phys. Rev. E* **69**, 036607 (2004)
50. G. Méchain, A. Couairon, Y.-B. André, C. D'amico, M. Franco, B. Prade, S. Tzortzakis, A. Mysyrowicz, and R. Sauerbrey, "Long-range self-channeling of infrared laser pulses in air: a new propagation regime without ionization," *Appl. Phys. B* **79**, 379-382 (2004)
51. J. Kasparian, Some properties of femtosecond laser filamentation relevant to atmospheric applications. Part I. The robustness of filamentation, in *Progress in Ultrafast Intense Laser Science II*, K. Yamanouchi, S. L. Chin, P. Agostini, G. Ferrante, Editors. 2007, Springer. p. 281-300.
52. J. Kasparian, Some properties of femtosecond laser filamentation relevant to atmospheric applications II. Large-scale filamentation, in *Progress in Ultrafast Intense Laser Science II*, K. Yamanouchi, S. L. Chin, P. Agostini, G. Ferrante, Editors. 2007, Springer. p. 301-318.
53. M. Mlejnek, E. M. Wright, J. V. Moloney, "Dynamic spatial replenishment of femtosecond pulses propagating in air," *Opt. Lett.* **23**, 382-384 (1998)
54. P. M. Goojrian, A. Taflove, R. M. Joseph, S. C. Hagness, "Computational modeling of femtosecond optical solutions from Maxwell equations," *IEEE J. Quantum Electron.* **28**, 2416-2422 (1992)
55. J. K. Ranka, A. L. Gaeta, "Breakdown of the slowly varying envelope approximation in the self-focusing of ultrashort pulses," *Opt. Lett.* **23**, 534-536 (1998).
56. A. Chiron, B. Lamouroux, R. Lange, J.-F. Ripoche, M. Franco, B. Prade, G. Bonnaud, G. Riazuelo, A. Mysyrowicz, "Numerical simulations of the nonlinear propagation of femtosecond optical pulses in gases," *The European Physical Journal D* **6**, 383-396 (1999)
57. N. Aközbe, C. M. Bowden, A. Talebour, S. L. Chin, "Femtosecond pulse propagation in air : variational analysis," *Phys. Rev. E* **61**, 4540-4549 (2000)
58. L. Hovhannisyann, "Analytic solution of the wave equation describing dispersion-free propagation of a femtosecond laser pulse in a medium with cubic and fifth-order nonlinearity," *Optics Commun.* **196**, 103-107 (2001)
59. P. Sprangle, J. R. Peñano and B. Hafizi, "Propagation of intense short laser pulses in the atmosphere," *Phys. Rev. E* **66**, 046418 (2002).
60. M. Kolesik, J. V. Moloney, "Nonlinear optical pulse propagation simulation: From Maxwell's to unidirectional equations," *Phys. Rev. E* **70**, 036604 (2004)
61. M. Mlejnek, M. Kolesik, J. V. Moloney, E. M. Wright, "Optically turbulent femtosecond light guide in air," *Phys. Rev. Lett.* **83**, 2938-2941 (1999)
62. Ren, R. G. Hemker, R. A. Fonseca, B. J. Duda, W. B. Mori, "Mutual attraction of laser beams in plasmas: braided light," *Phys. Rev. Lett.* **85**, 2124-2127 (2000).
63. G. Fibich, B. Ilan, "Deterministic vectorial effect lead to multiple filamentation," *Opt. Lett.* **26**, 840-842 (2001)
64. L. Bergé, S. Skupin, F. Lederer, G. Méjean, J. Yu, J. Kasparian, E. Salmon, J. P. Wolf, M. Rodriguez, L. Wöste, R. Bourayou, R. Sauerbrey, "Multiple filamentation of TW laser pulses in air," *Phys. Rev. Lett.* **92**, 225002 (2004)
65. S. A. Hosseini, Q. Luo, B. Ferland, W. Liu, S. L. Chin, O. G. Kosareva, N. A. Panov, N. Aközbe, V. P. Kandidov, "Competition of multiple filaments during the propagation of intense femtosecond laser pulses," *Phys. Rev. A*, **70**, 033802 (2004)
66. V. P. Kandidov, N. Akozbek, M. Scalora, O. G. Kosareva, A. V. Nyakk, Q. Luo, S. A. Hosseini, S. L. Chin, "Towards a control of multiple filamentation by spatial regularization of a high-power femtosecond laser pulse," *Appl. Phys. B* **80**, 267-275 (2005)
67. N. Blanchot, D. Le Goff, I. Le Goff, P. Manac'h, E. Mazataud, M. Nicolaizeau, M. Padois, L. Videau, D. Villate, L. Voisin, "A new versatile Nd:glass 200 J facility: ALISE; or from monochromatic and smoothed nanosecond pulses towards the ultra-intense femtosecond regime," *Conference on Laser and Electro-Optics, CWB4* (2002)
68. J. Kasparian, R. Sauerbrey, D. Mondelain, S. Niedermeier, J. Yu, J.-P. Wolf, Y.-B. André, M. Franco, B. Prade, A. Mysyrowicz, S. Tzortzakis, M. Rodriguez, H. Wille, L. Wöste, "Infrared extension of the supercontinuum generated by fs-TW-laser pulses propagating in the atmosphere," *Opt. Lett.* **25**, 1397-1399 (2000)
69. G. Méjean, J. Kasparian, J. Yu, S. Frey, E. Salmon, R. Ackermann, J.P. Wolf, L. Bergé, S. Skupin, "UV-Supercontinuum generated by long-range filamentation in air," *Appl. Phys. B* **82**, 341-345 (2006)
70. N. Aközbe, A. Iwasaki, A. Becker, M. Scalora, S. L. Chin C. M. Bowden, "Third-harmonic generation and self-channeling in air using high-power femtosecond laser pulses," *Phys. Rev. Lett.* **89**, 143901 (2002).

71. H. Yang, J. Zhang, J. Zhang, L. Z. Zhao, Y. J. Li, H. Teng, Y. T. Li, Z. H. Wang, Z. L. Chen, Z. Y. Wei, J. X. Ma, W. Yu and Z. M. Sheng, "Third-order harmonic generation by self-guided femtosecond pulses in air," *Phys. Rev. E* **67**, 015401 (2003).
72. W. Liu, S.A. Hosseini, Q. Luo, B. Ferland, S.L. Chin, O.G. Kosareva, N.A. Panov, and V. P. Kandidov, "Experimental observation and simulations of the self-action of white-light laser propagating in air," *New Journal of Physics*, **6**, 1-22 (2004)
73. S. L. Chin, S. Petit, F. Borne, K. Miyazaki, "The white light supercontinuum is indeed an ultrafast white light laser," *Japanese journal of Appl. Phys.* **38**, L126-L128 (1999)
74. O. G. Kosareva, V. P. Kandidov, A. Brodeur, C. Y. Chien, S. L. Chin, "Conical emission from laser-plasma interactions in the filamentation of powerful ultrashort laser pulses in air," *Chin. Opt. Lett.* **22**, 1332-1334 (1997).
75. T. J. Nibbering, P. F. Curley, G. Grillon, B. S. Prade, M. A. Franco, F. Salin, A. Mysyrowicz, "Conical emission from self-guided femtosecond pulses in air," *Opt. Lett.* **21**, 62-64 (1996).
76. J. Yu, D. Mondelain, G. Ange, R. Volk, S. Niedermeier, J.-P. Wolf, J. Kasparian, R. Sauerbrey, "Backward supercontinuum emission from a filament generated by ultrashort laser pulses in air," *Opt. Lett.* **26**, 533-535 (2001).
77. K. Strong, R.L. Jones, "Remote measurements of vertical profiles of atmospheric constituents with a UV-visible ranging spectrometer," *Appl. Opt.* **34**, 6223-6235 (1995)
78. J. Kasparian and J.-P. Wolf, "A new transient SRS analysis method of aerosols and application to a non-linear femtosecond Lidar," *Opt. Commun.* **152**, 355-360 (1998)
79. S. Spälter, N. Korolkova, F. König, A. Sizmann, G. Leuchs, "Observation of Multimode Quantum Correlations in Fiber Optical Solitons," *Phys. Rev. Lett.* **81**, 786-789, (1998)
80. T. Opatrny, N. Korolkova, and G. Leuchs, "Mode Structure and Photon Number Correlations in Squeezed Quantum Pulses," *Phys. Rev. A* **66**, 053813 (2002)
81. S. J. Carter, P. D. Drummond, M. D. Reid, R. M. Shelby, "Squeezing of quantum solitons," *Phys. Rev. Lett.* **58**, 1841-1844 (1987)
82. M. Rosenbluh and R. M. Shelby, "Squeezed optical solitons," *Phys. Rev. Lett.* **66**, 153-156 (1991)
83. K. Bergman and H. A. Haus, "Squeezing in fibers with optical pulses," *Opt. Lett.* **16**, 663-665 (1991)
84. K. Bergman, C. R. Doerr, H. A. Haus and M. Shirasaki, "Sub-shot-noise measurement with fiber squeezed optical pulses," *Opt. Lett.* **18**, 643-645 (1993)
85. K. Bergman, H. A. Haus, E. P. Ippen and M. Shirasaki, "Squeezing in a fiber interferometer with a gigahertz pump," *Opt. Lett.* **19**, 290-292 (1994)
86. N. Nishizawa, S. Kume, M. Mori, T. Goto and A. Miyauchi, "Squeezed light generation with 1.064  $\mu$ m Nd:YAG laser and 0.85  $\mu$ m single-mode fiber," *Jpn. J. Appl. Phys., Part 1* **33**, 138-143 (1994)
87. L. Boivin, F. X. Kärtner, H. A. Haus, "Analytical Solution to the Quantum Field Theory of Self-Phase Modulation with a Finite Response Time," *Phys. Rev. Lett.*, **73**, 240-243, (1994)
88. Mecozzi and P. Kumar, "Linearized quantum-fluctuation theory of spectrally-filtered optical solitons," *Opt. Lett.* **22**, 1232-1234 (1997)
89. V. Schmidt, L. Knöll, D.-G. Welsch, "Cumulant expansion for studying damped quantum solitons," *Phys. Rev. A* **59**, 2442-2457 (1999)
90. Pierre Béjot, Jérôme Kasparian, Estelle Salmon, Roland Ackermann, Nicolas Gisin, Jean-Pierre Wolf, "Laser Noise Reduction in Air," *Appl. Phys. Lett.* **88**, 251112 (2006)
91. P. Béjot, J. Kasparian, E. Salmon, R. Ackermann, J.-P. Wolf, "Spectral correlation and noise reduction in laser filaments," *Applied Physics B*, **87**, 1-4 (2007)
92. P. Béjot, C. Bonnet, V. Boutou, J.-P. Wolf, "Laser Noise Compression by Filamentation at 400 nm in Argon," *Opt. Express* **15**, 13295-13309 (2007)
93. G. P. Agrawal, *Nonlinear Fiber Optics*, Third Edition, Academic Press, p. 102 (1995)
94. J. H. Marburger, E. L. Dawes, "Dynamical formation of a small-scale filament," *Phys. Rev. Lett.* **21**, 556-558 (1968). Note that the radius considered in the classical writing of Marburger's formula is the half-width at  $e^{-1/2}$ , not  $1/e$  or  $1/e^2$  as usually.
95. J. Kasparian, M. Rodriguez, G. Méjean, J. Yu, E. Salmon, H. Wille, R. Bourayou, S. Frey, Y.-B. André, A. Mysyrowicz, R. Sauerbrey, J.-P. Wolf, L. Wöste, "White-Light Filaments for Atmospheric Analysis," *Science* **301**, 61-64 (2003).
96. T. Baumert, T. Brixner, V. Seyfried, M. Strehle, G. Gerber, "Femtosecond pulse shaping by an evolutionary algorithm with feedback," *Appl. Phys. B* **65**, 779-782 (1997)
97. G. Heck, J. Sloss, R.J. Levis, "Adaptative control of the spatial position of white light filaments in an aqueous solution," *Optics Communication*, **259**, 216-222 (2006)
98. D. Walter, S. Eyring, J. Lohreier, R. Spitzenpfeil, C. Spielmann, "Spatial optimization of filaments," *Appl. Phys. B* **88**, 175-178 (2007)
99. R. Ackermann, E. Salmon, N. Lascoux, J. Kasparian, P. Rohwetter, K. Stelmaszczyk, S. Li, A. Lindinger, L. Wöste, P. Béjot, L. Bonacina, J.-P. Wolf, "Optimal control of filamentation in air," *Appl. Phys. Lett.* **89**, 171117 (2006)
100. M. Fiorentino, J. E. Sharping, P. Kumar, A. Porzio, R. S. Windeler, "Soliton squeezing in microstructured fiber," *Opt. Lett.* **27**, 649-651 (2002)
101. S. Spälter, M. Burk, U. Ströbner, A. Sizmann, G. Leuchs, "Propagation of quantum properties of sub-picosecond solitons in a fiber," *Opt. Express*, **2**, 77-83 (1998)
102. S. R. Friberg, S. Machida, M. J. Werner, A. Levanon, T. Mukai, "Observation of Optical Soliton Photon-Number Squeezing," *Phys. Rev. Lett.* **77**, 3775-3778 (1996)

103. E.L. Dawes, J.H. Marburger, "Computer studies in self-focusing," *Phys. Rev.* **179**, 862-868 (1969)
104. G. Méchain, C. D'Amico, Y.-B. André, S. Tzortzakis, M. Franco, B. Prade, A. Mysyrowicz, A. Couairon, E. Salmon, R. Sauerbrey, "Range of plasma filaments created in air by a multi-terawatt femtosecond laser," *Opt. Commun.* **247**, 171-180 (2005)
105. I. S. Golubtsov, V. P. Kandidov, and O. G. Kosareva, "Initial phase modulation of a high-power femtosecond laser pulse as a tool for controlling its filamentation and generation of a supercontinuum in air," *Quantum Electronics.* **33**, 525-530 (2003)
106. V.P. Kandidov, N. Akosbek, M. Scarola, O.G. Kosareva, A.V. Nyakk, Q. Luo, S.A. Hosseini, S. L. Chin, "Towards a control of multiple filamentation by spatial regularization of a high-power femtosecond laser pulse," *Appl. Phys. B.* **80**, 267-275 (2005)
107. G. Fibich and B. Ilan, "Self-focusing of elliptic beams: an example of the failure of the aberrationless approximation," *J. Opt. Soc. Am.* **17**, 1749-1758 (2000)
108. S. Skupin, L. Bergé, U. Peschel, F. Lederer, G. Méjean, J. Yu, J. Kasparian, E. Salmon, J.P. Wolf, M. Rodriguez, L. Wöste, R. Bourayou, R. Sauerbrey, "Filamentation of femtosecond light pulses in the air: Turbulent cells versus long-range clusters," *Phys. Rev. E* **70**, 046602 (2004)
109. H. Yang, J. Zhang, Q. Zhang, Z. Hao, Y. Li, Z. Zheng, Z. Wang, Q.-L. Dong, X. Lu, Z. Wei, Z.-M. Sheng, J. Yu, W. Yu, "Polarization-dependent supercontinuum generation from light filaments in air," *Opt. Lett.* **30**, 534-536 (2005)
110. S. Judson and H. Rabitz, "Teaching lasers to control molecules," *Phys. Rev. Lett.* **68**, 1500-1503 (1992)
111. D. Goswami, "Optical pulse shaping approaches to coherent control," *Phys. Rep.* **374**, 385-481 (2003), and references therein
112. M. Dantus, V. V. Lozovoy, "Experimental coherent laser control of physicochemical processes," *Chemical Reviews* **104**, 1813-1859 (2004), and references therein
113. T. Back, H.P. Schwefel, "An overview of evolutionary algorithms for parameter optimization," *Evolutionary Computing* **1**, 1-23 (1993)
114. Luigi Bonacina, Jérôme Extermann, Ariana Rondi, Véronique Boutou, Jean-Pierre Wolf, "Multiobjective genetic approach for optimal control of photoinduced processes," *Phys. Rev. A* **76**, 023408 (2007)
115. A. Bartelt, S. Minemoto, C. Lupulescu, S. Vajda, L. Wöste, "Control of wavepacket dynamics in mixed alkali metal clusters by optimally shaped fs pulses," *European Physical Journal D* **16**, 127-131 (2001)
116. J. Yu, D. Mondelain, J. Kasparian, E. Salmon, S. Geffroy, C. Favre, V. Boutou, J.P. Wolf, "Sonographic probing of laser filaments in air," *Appl. Opt.* **42**, 7117-7120 (2003)
117. Y.T. Li, J. Zhang, H. Teng, K. Li, X.Y. Peng, Z. Jin, X. Lu, Z.Y. Zheng, and Q.Z. Yu, "Blast wave produced by interactions of femtosecond laser pulses with water," *Phys. Rev. E.* **67**, 056403 (2003)
118. S.A. Hosseini, J. Yu, Q. Luo, and S.L. Chin, "Multi-parameter characterization of the longitudinal plasma profile of a filament: a comparative study," *Appl. Phys. B.* **79**, 519-523 (2004)
119. D. Schumacher, "Controlling continuum generation," *Opt. Lett.* **27**, 451-453 (2002)
120. G. Méjean, J. Kasparian, J. Yu, S. Frey, E. Salmon, and J.-P. Wolf, "Remote Detection and Identification of Biological Aerosols using a Femtosecond Terawatt Lidar System," *Appl. Phys. B.* **78**, 535-537 (2004)
121. K. Stelmaszczyk, P. Rohwetter, G. Méjean, J. Yu, E. Salmon, J. Kasparian, R. Ackermann, J.-P. Wolf, L. Wöste, "Long-distance remote laser-induced breakdown spectroscopy using filamentation in air," *Appl. Phys. Lett.* **85**, 3977-3979 (2004)
122. P. Rohwetter, J. Yu, G. Méjean, K. Stelmaszczyk, E. Salmon, J. Kasparian, J.-P. Wolf, and L. Wöste, "Remote LIBS with ultra-short pulses: characteristics in picosecond and femtosecond regimes," *Journal of analytical atomic spectrometry.* **19**, 437-444 (2004)
123. Y. Shverdin, S. N. Goda, G. Y. Yin, S. E. Harris, "Coherent control of laser-induced breakdown," *Opt. Lett.* **31**, 1331-1333 (2006)
124. L. Iorio, H. Lichtenegger, B. Mashhoon, "An alternative derivation of the gravitomagnetic clock effect," *Classical and Quantum Gravity* **19**, 39-49 (2002)
125. F. Courvoisier, V. Boutou, J. Kasparian, E. Salmon, G. Méjean, J. Yu et J. P. Wolf, "Light filaments transmitted through clouds," *Appl. Phys. Lett.* **83**, 213-215 (2003)
126. M. Mlejnek, E. M. Wright, J. V. Moloney, "Power dependence of dynamic spatial replenishment of femtosecond pulses propagating in air," *Opt. Express* **4**, 223-228 (1999).
127. M. Kolesik, J. V. Moloney, "Self-healing femtosecond light filaments," *Opt. Lett.* **29**, 590-590 (2004)
128. S. Skupin, L. Bergé, U. Peschel, F. Lederer, "Interaction of femtosecond light filaments with obscurants in aerosols," *Phys. Rev. Lett.* **93**, 023901 (2004)
129. S. L. Chin, A. Brodeur, S. Petit, O. G. Kosareva, V. P. Kandidov, "Filamentation and supercontinuum generation during the propagation of powerful ultrashort laser pulses in optical media (white light laser)," *Journal of Nonlinear Optical Physics and Materials* **8**, 121-146 (1999)
130. W. Liu, J.F. Gravel, F. Théberge, A. Becker, S.L. Chin, "Background reservoir: its crucial role for long-distance propagation of femtosecond laser pulses in air," *Appl. Phys. B* **80**, 857-860 (2005)
131. S. Skupin, L. Bergé, U. Peschel, and F. Lederer, "Interaction of femtosecond light filaments with obscurants in aerosols," *Phys. Rev. Lett.* **93**, 023901 (2004)
132. G. Méchain, G. Méjean, R. Ackermann, P. Rohwetter, Y.-B. André, J. Kasparian, B. Prade, K. Stelmaszczyk, J. Yu, E. Salmon, W. Winn, L. A. Schlie, A. Mysyrowicz, R. Sauerbrey, L. Wöste, and J.-P. Wolf, "Propagation of fs-TW laser filaments in adverse atmospheric conditions," *Appl. Phys. B.* **80**, 785-789 (2005)
133. V. I. Tatarski, *The effects of the Turbulent Atmosphere on Wave Propagation* (Keter, Jerusalem, 1971)

134. S. Bendersky, N. S. Kopeika, N. Blaunstein, "Atmospheric optical turbulence over land in Middle-East coastal environments: prediction modeling and measurements," *Appl. Opt.* **43**, 4070-4079 (2004)
135. S. L. Chin, A. Talebpoor, J. Yang, S. Petit, V. P. Kandidov, O. G. Kosareva, M. P. Tamarov, "Filamentation of femtosecond laser pulses in turbulent air," *Appl. Phys. B* **74**, 67-76 (2002)
136. P. Rambo, J. Schwartz, J.-C. Diels, "High-voltage electrical discharges induced by an ultrashort-pulse UV laser system," *J. Opt. A: Pure and Appl. Opt.* **3**, 146-158 (2001)
137. S. A. Shlyonov and V. P. Kandidov, "Filament bunch formation upon femtosecond laser pulse propagation through the turbulent atmosphere. Part 1. Method," *Atmos. Oceanic Opt.* **17**, 565-570 (2004)
138. S. A. Shlyonov and V. P. Kandidov, "Filament bunch formation upon femtosecond laser pulse propagation through the turbulent atmosphere. Part 2. Statistical characteristics," *Atmos. Oceanic Opt.* **17**, 571-575 (2004)
139. R. Ackermann, G. Méjean, J. Kasparian, J. Yu, E. Salmon, J.-P. Wolf, "Laser filaments generated and transmitted in highly turbulent air," *Opt. Lett.* **31**, 86-88 (2006)
140. R. Salamé, N. Lascoux, E. Salmon, R. Ackermann, J. Kasparian, "Propagation of laser filaments through an extended turbulent region," *Appl. Phys. Lett.* **91**, 171106 (2007)
141. G. Méjean, J. Kasparian, E. Salmon, J. Yu, J.-P. Wolf, R. Bourayou, R. Sauerbrey, M. Rodriguez, L. Wöste, H. Lehmann, B. Stecklum, U. Laux, J. Eisloffel, A. Scholz, and A.P. Hatzes, "Towards a supercontinuum-based infrared Lidar," *Appl. Phys. B* **77**, 357-359 (2003)
142. L. S. Rothman, A. Barbe, D. C. Benner, L. R. Brown, C. Camy-Peyret, M. R. Carleer, K. Chance, C. Clerbaux, V. Dana, V. M. Devi, A. Fayt, J.-M. Flaud, R. R. Gamache, A. Goldman, D. Jacquemart, K. W. Jucks, W. J. Lafferty, J.-Y. Mandin, S. T. Massie, V. Nemtchinov, D. A. Newnham, A. Perrin, C. P. Rinsland, J. Schroeder, K. M. Smith, M. A. H. Smith, K. Tang, R. A. Toth, J. Vander Auwera, P. Varanasi and K. Yoshino, "The HITRAN Molecular Spectroscopic Database: Edition of 2000 Including Updates of 2001," *Journal of quantitative spectroscopy and radiation transfer* **82**, 5 (2003)
143. R. Bourayou, G. Méjean, J. Kasparian, M. Rodriguez, E. Salmon, J. Yu, H. Lehmann, B. Stecklum, U. Laux, J. Eisloffel, A. Scholz, A.P. Hatzes, R. Sauerbrey, L. Wöste, J.-P. Wolf, "White-light filaments for multiparameter analysis of cloud microphysics," *J. Opt. Soc. Am. B* **22**, 369-377 (2005)
144. G. Mégie, "Mesure de la pression et de la température atmosphériques par absorption différentielle lidar: influence de la largeur d'émission laser," *Appl. Opt.* **19**, 34-43 (1980)
145. H. Müller, H. Quenzel, "Information content of multispectral Lidar measurements with respect to the aerosol size distribution," *Appl. Opt.* **24**, 648-654 (1985)
146. P.-H. Wang, M. P. McCormick, M. T. Osborn, W. H. Fuller, "Stratospheric aerosol model size distributions derived from multiwavelength lidar observations," 14th International Laser Radar Conference, San Candido, Italy (1988)
147. L. Stefanutti, M. Castagnoli, M. Del Guasta, M. Morandi, V. M. Sacco, V. Venturi, L. Zuccagnoli, J. Kolenda, H. Kneipp, P. Rairoux, B. Stein, D. Weidauer, J. P. Wolf, "A four wavelength depolarization backscattering Lidar for polar stratospheric cloud monitoring," *Appl. Phys. B* **55**, 13-17 (1992)
148. Y. S. Kim, Y. Iwasaka, G. Y. Shi, T. Nagatani, T. Shibata, D. Trochkin, A. Matsuki, M. Yamada, B. Chen, D. Zhang, M. Nagatani, H. Nakata, "Dust particles in the free atmosphere over desert areas on the Asian continent: Measurements from summer 2001 to summer 2002 with balloon-borne optical particle counter and lidar, Dunhuang, China," *J. Geophys. Res.-Atmospheres* **109** (D19), D9S26 (2004)
149. J. Redemann, R. P. Turco, R. F. Pueschel, M. A. Fenn, E. V. Browell, W. B. Grant, "A multi-instrument approach for characterizing the vertical structure of aerosol properties: case studies in the Pacific Basin troposphere," *J. Geophys. Res. - Atmospheres* **103** (D18): 23287-23298 (1998)
150. M.C. Galvez, M. Fujita, N. Inoue, R. Moriki, Y. Izawa, C. Yamanaka, "Three-wavelength backscatter measurement of clouds and aerosols using a white light Lidar system," *Jap. J. App. Phys.* **41**, 284 (2002)
151. G. Faye, J. Kasparian, R. Sauerbrey, "Modifications to the Lidar equation due to nonlinear propagation in air," *Appl. Phys. B* **73**, 157-163 (2001)
152. S. R. Pal and A. I. Carswell, "Multiple scattering in atmospheric clouds: Lidar observations," *Appl. Opt.* **15**, 1990-1995 (1976)
153. J. S. Ryan, S. R. Pal, A. I. Carswell, "Laser backscattering from dense water-droplet clouds," *J. Opt. Soc. Am.* **69**, 60-67 (1979)
154. L. R. Bissonnette and D. L. Hutt, "Multiply scattered aerosol lidar returns: inversion method and comparison with in-situ measurements," *Appl. Opt.* **34**, 6959-6975 (1995)
155. L. R. Bissonnette, "Multiple-scattering Lidar equation," *Appl. Opt.* **35**, 6449-6465 (1996)
156. V. Korolev, G. A. Isaac, I. P. Mazin, H. W. Barker, "Microphysical properties of continental clouds from in situ measurements," *Quarterly Journal of the Royal meteorological society* **127**, 2117-2151 (2001)
157. L. Miles, J. Verlinde, E. E. Clothiaux, "Cloud droplet size distributions in low-level stratiform clouds," *Journal of the atmospheric sciences* **57**, 295-311 (2000)
158. J.-P. Wolf, Y.-L. Pan, G. Turner, M.C. Beard, C.A. Schmittenmaer, S. Holler, R.K. Chang, "Ballistic trajectories of optical wave packets within microcavities," *Phys. Rev. A* **64**, 023808 (2001).
159. L. Méès, J.P. Wolf, G. Gouesbet, G. Gréhan, "Two-photon absorption and fluorescence in a spherical micro-cavity illuminated by using two laser pulses: numerical simulations," *Optics Comm.* **208**, 371-375 (2002)
160. V. Boutou, C. Favre, S.C. Hill, Y.L. Pan, R.K. Chang, J.-P. Wolf, "Backward enhanced emission from multiphoton processes in aerosols," *Appl. Phys. B* **75**, 145-152 (2002)
161. S.C. Hill, V. Boutou, J. Yu, S. Ramstein, J.-P. Wolf, Y.-L. Pan, S. Holler, R.K. Chang, "Enhanced backward-directed multiphoton-excited fluorescence from dielectric microspheres," *Phys. Rev. Lett.* **85**, 54-57 (2000).

162. C. Favre, V. Boutou, S. C. Hill, W. Zimmer, M. Krenz, H. Lambrecht, J. Yu, R. K. Chang, L. Wöste, J.-P. Wolf, "White-light nanosource with directional emission," *Phys. Rev. Lett.* **89** 035002 (2002)
163. F. Williams, D.P. Warma, S. Hillenius, "Liquid water as a lone-pair amorphous semiconductor," *J. Chem. Phys.* **64**, 1549-1554 (1976).
164. J. Noack, A. Vogel, "Laser-induced plasma formation in water at nanosecond to femtosecond time scales: Calculation of thresholds, absorption coefficients, and energy density," *IEEE J. Quantum Electron.* **35**, 1156-1167 (1999).
165. Y. Pan, S. C. Hill, J.P. Wolf, S. Holler, R.K. Chang, J.R. Bottiger, "Backward-enhanced fluorescence from clusters of microspheres and particles of tryptophan," *Appl. Opt.* **41**, 2994-2999 (2002)
166. Y. Pan, S. Holler, R.G. Pinnick, S. C. Hill, S. Niles, J.R. Bottiger, J.P. Wolf, R. K. Chang, "Dynamics of photon-induced degradation and fluorescence in riboflavin microparticles," *App. Phys. B* **72**, 449-454 (2001)
167. S.C. Hill, R. Pinnick, S. Niles, Y.L. Pan, S. Holler, R.K. Chang, J. Bottiger, B.T. Chen, C.S. Orr, G. Feather, "Real-time measurement of fluorescence spectra from single airborne biological particles," *Field Analytical Chemistry and Technology* **3**, 221-239 (1999)
168. G.W. Faris, R. A. Copeland, K. Mortelmans, B. V. Bronk, "Spectrally resolved absolute fluorescence cross sections for bacillus spores," *Appl. Opt.* **36**, 958-967 (1997)
169. R.M. Measures, *Laser Remote Sensing, Fundamentals and Applications* (J. Wiley and Sons, New York, 1984).
170. A. Iwasaki, N. Aközbe, B. Ferland, Q. Luo, G. Roy, C.M. Bowden, S.L. Chin, "A LIDAR technique to measure the filament length generated by a high-peak power femtosecond laser pulse in air," *Appl. Phys. B* **76**, 231-236 (2003)
171. Q. Luo, S. A. Hosseini, B. Ferland and S. L. Chin, "Backward time-resolved spectroscopy from filament induced by ultrafast intense laser pulses," *Opt. Commun.* **233**, 411-416 (2004)
172. J.-F. Gravel, Q. Luo, D. Boudreau, X. P. Tang, S. L. Chin, "Sensing of Halocarbons Using Femtosecond Laser-Induced Fluorescence," *Anal. Chem.* **76**, 4799-4805 (2004)
173. Q. Luo, H.L. Xu, S.A. Hosseini, J.-F. Daigle, F. Théberge, M. Sharifi, S.L. Chin, "Remote sensing of pollutants using femtosecond laser pulse fluorescence spectroscopy," *Appl. Phys. B-Lasers and Optics.* **82**, 105-109 (2006)
174. P. Rosch, M. Harz, M. Schmitt, K-D Peschke, O. Ronneberger, H. Burkhardt, H-W Motzkus, M. Lankers, S. Hofer, H. Thiele, J. Popp, "Chemotaxonomic Identification of Single Bacteria by Micro-Raman Spectroscopy: Application to Clean-Room-Relevant Biological Contaminations," *Applied and environmental microbiology* **71**, 1626-1637 (2005); and references therein
175. D. Pestov, R. K. Murawski, G. O. Ariunbold, X. Wang, M. Zhi, A.V. Sokolov, V. A. Sautenkov, Y. V. Rostovtsev, A. Dogariu, Y. Huang, M. O. Scully, "Optimizing the Laser-Pulse Configuration for Coherent Raman Spectroscopy," *Science* **316**, 265-268 (2007)
176. M. O. Scully, G. W. Kattawar, R. P. Lucht, T. Opatrny, H. Pilloff, A. Z. Sokolov, M. S. Zubairy, "FAST CARs: Engineering a laser spectroscopic technique for rapid identification of bacterial spores," *Proceedings of the National Academy of Sciences* **99**, 10994-11001 (2002)
177. K. Talaro, A. Talaro, *Foundations of Microbiology*, W.C. Brown Publ., Dubuque, IA (1999)
178. Special issue on femtosecond coherent Raman spectroscopy, W. Kiefer, Editor, *J. Raman Spectroscopy* **31**, 1-144 (2000),
179. D. Oron, N. Dudovich, D. Yelin, Y. Silberberg, "Quantum control of coherent anti-Stokes Raman processes" *Phys. Rev. A* **65**, 043408 (2002)
180. D. Oron, N. Dudovich, Y. Silberberg, "Single-pulse phase-contrast nonlinear Raman spectroscopy," *Phys. Rev. Lett.* **89** 273001 (2002)
181. N. Dudovich, D. Oron, Y. Silberberg, "Single-pulse coherently controlled nonlinear Raman spectroscopy and microscopy," *Nature* **418** (6897): 512-514 (2002)
182. M. Baudelet, L. Guyon, J. Yu, J.P. Wolf, T. Amodeo, E. Fréjafon, P. Laloi, "Spectral signature of native CN bonds for bacterium detection and identification using femtosecond laser-induced breakdown spectroscopy," *Appl. Phys. Lett.* **88**, 063901 (2006)
183. M. Baudelet, L. Guyon, J. Yu, J.-P. Wolf, T. Amodeo, E. Fréjafon, P. Laloi, "Femtosecond Laser-Induced Breakdown Spectroscopy of Escherichia Coli: Atomic and Molecular Spectroscopic Markers of the Bacterium," *Appl. Phys. Lett.* **88**, 053901 (2006)
184. M. Baudelet, J. Yu, M. Bossu, J. Jovelet, J.-P. Wolf, T. Amodeo, E. Fréjafon, P. Laloi, "Discrimination of Microbiological Samples using Femtosecond Laser-induced Breakdown Spectroscopy," *Appl. Phys. Lett.* **89**, 163903 (2006)
185. S. Palanco, L.M. Cabalin, D. Romero, J. J. Laserna, "Infrared laser ablation and atomic emission spectrometry of stainless steel at high temperatures," *J. Anal. At. Spectrom.*, **14**, 1883-1887 (1999)
186. S. Palanco, S. Conesa, J. J. Laserna, "Field deployable or remote enabled? A portable laser-induced plasma spectrometer for field remote sensing," Paper presented at EMSLIBS, Hersonissos, Greece, September 2003
187. Ph. Rohwetter, K. Stelmasczyk, L. Wöste, R. Ackermann, G. Méjean, E. Salmon, J. Kasparian, J. Yu and J.P. Wolf, "Filament-induced Remote Ablation for Long Range LIBS Operation," *Spectrochimica Acta B* **60**, 1025-1033 (2005)
188. Ph. Rohwetter, J. Yu, G. Méjean, K. Stelmasczyk, E. Salmon, J. Kasparian, J.P. Wolf, L. Wöste, "Remote LIBS with Ultra-Short Pulses: Characteristics in Picosecond and Femtosecond Regimes," *J. of Anal. Atomic Spect.* **19**, 437-444 (2004)

189. H. L. Xu, G. Méjean, W. Liu, Y. Kamali, J.-F. Daigle, A. Azarm, P. T. Simard, P. Mathieu, G. Roy, J.-R. Simard, S. L. Chin, "Remote detection of similar biological materials using femtosecond filament-induced breakdown spectroscopy," *Appl. Phys. B*, **87**, 151-156 (2007)
190. W. Liu, H. L. Xu, G. Méjean, Y. Kamali, J.-F. Daigle, A. Azarm, P. T. Simard, P. Mathieu, G. Roy, S. L. Chin, "Efficient non-gated remote filament-induced breakdown spectroscopy of metallic sample," *Spectrochimica Acta B-Atomic Spectroscopy* **62**, 76-81 (2007)
191. H. L. Xu, Y. Kamali, C. Marceau, P. T. Simard, W. Liu, J. Bernardt, G. Méjean, P. Mathieu, G. Roy, J. R. Simard, S. L. Chin, "Simultaneous detection and identification of multigas pollutants using filament-induced nonlinear spectroscopy," *Appl. Phys. Lett.* **90**, 101106 (2007)
192. H. L. Xu, J. Bernardt, P. Mathieu, G. Roy, S. L. Chin, "Understanding the advantage of remote femtosecond laser-induced breakdown spectroscopy of metallic targets," *J. Appl. Phys.* **101**, 033124 (2007)
193. J.-F. Daigle, G. Méjean, W. Liu, F. Théberge, H. L. Xu, Y. Kamali, J. Bernardt, A. Azarm, A. Sun, P. Mathieu, G. Roy, J. R. Simard, S. L. Chin, "Long range trace detection in aqueous aerosol using remote filament-induced breakdown spectroscopy," *Appl. Phys. B* **87**, 749-754 (2007)
194. R. G. Pinnick, S. C. Hill, Y. L. Pan, R. K. Chang, "Fluorescence spectra of atmospheric aerosol at Adelphi, Maryland, USA: measurement and classification of single particles containing organic carbon," *Atmospheric Environment* **38**, 1657-1672 (2004)
195. F. Courvoisier, V. Boutou, V. Wood, J.P. Wolf, A. Bartelt, M. Roth, H. Rabitz, "Femtosecond laser pulses distinguish bacteria from background urban aerosols," *Appl. Phys. Lett.* **87**, 063901 (2005)
196. L. Sobolewski, W. Domcke, C. Dedonder-Lardeux, C. Jouvet, "Excited-state hydrogen detachment and hydrogen transfer driven by repulsive ( $1\pi$ ) sigma\* states: A new paradigm for nonradiative decay in aromatic biomolecules," *Phys. Chem. Chem. Phys.* **4**, 1093-1100 (2002)
197. H. B. Steen, "Wavelength dependence of quantum yield of fluorescence and photoionization of indoles," *J. Chem. Phys.* **61**, 3997-4002 (1974)
198. B. Q. Li, H. Rabitz, J. P. Wolf, "Optimal dynamic discrimination of similar quantum systems with time series data," *J. Chem. Phys.* **122**, 154103 (2005)
199. J. Extermann, P. Bejot, L. Bonacina, P. Billaud, J. Kasparian, J.-P. Wolf, "Effects of Atmospheric Turbulence on Remote Optical Control Experiments," to be published in *Appl. Phys. Lett.*
200. P. Hubert, "Triggered lightning in France and New Mexico," *Endeavour* **8**, 85-89 (1984)
201. A. Eybert-Bérard, C. Leteinturier, "Déclenchement artificiel de la foudre : moyens d'essais et mesures électriques," *Revue Générale d'Électricité*, n° 3 (Mars), 25 (1989)
202. D.W. Koopman, T. D. Wilkerson, "Channeling of an ionizing electrical streamer by a laser beam," *J. Appl. Phys.* **42**, 1883 (1971)
203. L. M. Ball, "The laser lightning rod system: thunderstorm domestication," *Appl. Opt.* **13**, 2292-2296 (1974)
204. M. Miki, Y. Aihara, T. Shindo, "Development of long gap discharges guided by a pulsed CO<sub>2</sub> laser," *J. Phys. D - Appl. Phys.* **26**, 1244-1252 (1993)
205. H. Pépin, D. Comtois, F. Vidal, C. Y. Chien, A. Desparois, T. W. Johnston, J. C. Kieffer, B. La Fontaine, F. Martin, F. A. M. Rizk, C. Potvin, P. Couture, H. P. Mercure, A. Bondiou-Clergerie, P. Lalande, I. Gallimberti, "Triggering and guiding high-voltage large-scale leader discharges with sub-joule ultrashort laser pulses," *Phys. Plasmas* **8**, 2532-2539 (2001)
206. D. Comtois, C. Y. Chien, A. Desparois, F. Gérin, G. Jarry, T. W. Johnston, J. C. Kieffer, B. La Fontaine, F. Martin, M. Mawassi, H. Pépin, F. A. M. Rizk, F. Vidal, P. Couture, H. P. Mercure, C. Potvin, A. Bondiou-Clergerie, I. Gallimberti, "Triggering and guiding leader discharges using a plasma channel created by an ultrashort laser," *Appl. Phys. Letters* **76**, 819-821 (2000)
207. M. Rodriguez, R. Sauerbrey, H. Wille, L. Wöste, T. Fujii, Y.-B. André, A. Mysyrowicz, L. Klingbeil, K. Rethmeier, W. Kalkner, J. Kasparian, E. Salmon, J. Yu, and J.-P. Wolf, "Megavolt discharges triggered and guided with laser filaments," *Opt. Lett.* **27**, 772-774 (2002)
208. R. Ackermann, G. Méchain, G. Méjean, R. Bourayou, M. Rodriguez, K. Stelmaszczyk, J. Kasparian, J. Yu, E. Salmon, S. Tzortzakis, Y.-B. André, J.-F. Bourrillon, L. Tamin, J.-P. Cascelli, C. Davoise, A. Mysyrowicz, R. Sauerbrey, L. Wöste, J.-P. "Wolf, Influence of negative leader propagation on the triggering and guiding of high voltage discharges by laser filaments," *Appl. Phys. B*, **82**, 561-566 (2006)
209. R. Ackermann, K. Stelmaszczyk, P. Rohwetter, G. Méjean, E. Salmon, J. Yu, J. Kasparian, G. Méchain, V. Bergmann, S. Schaper, B. Weise, T. Kumm, K. Rethmeier, W. Kalkner, J.P. Wolf, and L. Wöste, "Triggering and guiding of megavolt discharges by laser-induced filaments under rain conditions," *Appl. Phys. Lett.* **85**, 5781-5783 (2004)
210. Z. Hao, J. Zhang, Y.T. Li, X. Lu, X.H. Yuan, Z.Y. Zheng, Z.H. Wang, W.J. Ling, Z.Y. Wei, "Prolongation of the fluorescence lifetime of plasma channels in air induced by femtosecond laser pulses," *Applied Physics B* **80**, 627-630 (2005)
211. G. Méjean, R. Ackermann, J. Kasparian, E. Salmon, J. Yu, J.-P. Wolf, K. Rethmeier, W. Kalkner, P. Rohwetter, K. Stelmaszczyk, and L. Wöste, "Improved laser triggering and guiding of megavolt discharges with dual fs-ns pulses," *Appl. Phys. Lett.* **88**, 021101 (2006)
212. S. Tzortzakis, G. Méchain, G. Patalano, Y.-B. André, B. Prade, M. Franco, A. Mysyrowicz, J.-M. Munier, M. Gheudin, G. Beaudin, P. Encrenaz, "Coherent subterahertz radiation from femtosecond infrared filaments in air," *Opt. Lett.* **27**, 1944-1946 (2002)
213. G. Méchain, S. Tzortzakis, B. Prade, M. Franco, A. Mysyrowicz, B. Leriche, "Calorimetric detection of THz radiation from femtosecond filaments in air," *Appl. Phys. B* **77**, 707-709 (2003)

214. A. Houard, C. D'Amico, M. Franco, B. Prade, A. Mysyrowicz, A. Couairon, V. Tikhonchuk, "Cerenkov THz emission from femtosecond filamentation in air," CLEO/QELS Conference. Optical Society of America, Baltimore (2007)
215. C. D'Amico, A. Houard, M. Franco, B. Prade, A. Mysyrowicz, A. Couairon, V. T. Tikhonchuk, "Conical Forward THz Emission from Femtosecond-Laser-Beam Filamentation in Air," Phys. Rev. Lett., **98**, 235002 (2007)
216. C. D'Amico, B. Prade, M. Franco, A. Mysyrowicz, "Femtosecond filament amplification in liquids," Appl. Phys. B **85**, 49-53 (2006)
217. C.-C. Cheng, E. M. Wright, J. V. Moloney, "Generation of electromagnetic pulses from plasma channels induced by femtosecond light strings," Phys. Rev. Lett. **87**, 213001 (2001)
218. S. Tzortzakis, G. Méchain, G. Patalano, M. Franco, B. Prade, A. Mysyrowicz, "Concatenation of plasma filaments created in air by femtosecond infrared laser pulses," Appl. Phys. B **76**, 609-612 (2003)
219. S.A. Hosseini, Q. Luo, B. Ferland, W. Liu, N. Akösbek, G. Roy, and S.L. Chin, "Effective length of filaments measurement using backscattered fluorescence from nitrogen molecules," Appl. Phys. B. **77**, 697-702 (2003)
220. S. Tzortzakis, M.A. Franco, Y.-B. André, A. Chiron, B. Lamouroux, B.S. Prade, A. Mysyrowicz, "Formation of a conducting channel in air by self-guided femtosecond laser pulses," Phys. Rev. E. **60**, R3505-R3507 (1999)
221. E. Dormidonov, V. V. Valuev, V. L. Dmitriev, S. A. Shlenov, V. P. Kandidov, "Laser Filament Induced Microwave Waveguide in Air," ICONO/LAT conference 2007, Minsk, Belarus
222. C. Hönninger, R. Paschotta, M. Graf, F. Morier-Genoud, G. Zhang, M. Moser, S. Biswal, J. Nees, A. Braun, G.A. Mourou, I. Johannsen, A. Giesen, W. Seeber, U. Keller, "Ultrafast ytterbium-doped bulk lasers and laser amplifiers," Appl. Phys. B **69**, 3-17 (1999).
223. A. A. Lagatsky, C. T. A. Brown, W. Sibbett, "Highly efficient and low threshold diode-pumped Kerr-lens mode-locked Yb:KYW laser," Opt. Express **12**, 3928-3933 (2004)
224. A. Dubietis, G. Jonusauskas, A. Piskarskas, "Powerful femtosecond pulse generation by chirped and stretched pulse parametric amplification in BBO crystal," Opt. Commun. **88**, 437-440 (1992)
225. M. J. Guardalben, J. Keegan, L. J. Waxer, V. Bagnoud, I. A. Begishev, J. Puth, J. D. Zuegel, "Design of a highly stable, high-conversion-efficiency, optical parametric chirped-pulse amplification system with good beam quality," Opt. Express **11**, 2511-2524, (2003)

## 1. Introduction

High power laser pulses undergo nonlinear propagation in transparent media. Nonlinear self-action leads to strong evolutions of the spatial (self focusing [1,2], self guiding [3], self reflection [4]), spectral (four wave mixing [5], self phase modulation [6,7,8]) as well as temporal (self steepening [9,10,11], pulse splitting [12]) characteristics of the pulse. The propagation medium is also affected, as it is partially ionized by the propagating laser beam [13,14,15,16]. Those phenomena have been extensively studied since the early 1970's, from the theoretical as well as from the experimental points of view. But they were initially restricted to condensed matter, especially glass, where the damage associated with light filamentation prevented application.

Since 1985, the development of the chirped pulse amplification (CPA) technique [17,18] permitted to produce ultrashort laser pulses with intensities as high as  $10^{20}$  W/cm<sup>2</sup> and hence to observe highly nonlinear propagation even in slightly nonlinear media such as atmospheric pressure gases, including the atmosphere itself. The atmospheric propagation is much richer, and consequently much more complex than its counterpart at the laboratory scale [19], setting this field of research as one of the new frontiers of non-linear optics. However, this complexity is worth tackling, since it opens the way to many atmospheric applications in fields as diverse as lightning control and remote sensing of air pollution by Lidar (Light Detection and Ranging).

The Lidar technique has become a method of choice for obtaining 3D-profiles of atmospheric trace gases and aerosols. In particular, DIAL (Differential Absorption Lidar) has been extensively used to measure the spatial distributions of tropospheric pollutants like NO<sub>x</sub> [20,21], SO<sub>2</sub>, and O<sub>3</sub> [19,22,23,24]. The method has been widely applied for the understanding of tropospheric ozone and smog formation. It is particularly well suited for validating large-scale numerical simulations [25,26]. Lidar-DIAL systems are based on highly reliable solid-state lasers and have sensitivities in the ppb-range over several kilometers. However, the palette of detectable pollutants is strongly restricted by the availability of

powerful lasers, tunable over wide spectral ranges, and by spectral interference between the components. This limited investigations to the UV (225-400 nm), and to the related absorbing pollutants such as NO, NO<sub>2</sub>, SO<sub>2</sub>, O<sub>3</sub>, Hg, Benzene, and Toluene. Some results in the mid-IR using OPOs and DFM (Difference Frequency Mixing) have been reported for methane, while other VOC (Volatile Organic Compounds) could not be separated because of spectral overlapping [27]. Some original methods were proposed to combine spectrally resolved detection and broadband laser emission, but their application remained limited by the narrow laser bandwidth available [28,29].

Obtaining relevant information about aerosols (such as size distribution, composition) is a key subject in the Lidar research field. For example, during the arctic campaigns EASOE (1991-1992) and SESAME (1993-1994), sulfate aerosols injected in the stratosphere by the Mount Pinatubo eruption could clearly be distinguished from the size distribution of PSCs using 4-wavelength Lidars [30,31,32]. However, the determination of the aerosol size distribution in these experiments was based on a *a priori* postulated log-normal shape, for which the mean value, standard deviation and concentration were fitted using the Lidar data. Experiments have also been performed on tropospheric aerosols, using a combined Lidar—SEM-Microscopy—X-Ray-micronalysis method [33].

In spite of the great success of Lidar for monitoring the atmosphere, it remains limited today by the following drawbacks:

- ~ Since the principle of operation of conventional Lidar systems is based on quasi-isotropic scattering processes like Rayleigh, Mie, Raman and fluorescence, only a very small fraction of the signal is captured by the receiver, limiting the sensitivity for trace gases at large distance
- ~ The palette of selectively detectable species is restricted due to the lack of powerful tunable light sources in particular in the infrared. As a result only some substances that exhibit pronounced UV-transitions like NO<sub>2</sub>, O<sub>3</sub> or SO<sub>2</sub> are easily detectable, while organic trace gases remain virtually unreachable.
- ~ As a pair of fixed DIAL wavelengths is sent into the atmosphere, only one pollutant can be detected at a time, which has to be chosen prior to the measurement.
- ~ The DIAL-detection scheme is sensitive to overlapping spectra, and thus subject to interference between pollutants
- ~ Lidar probing in the IR is usually restricted to aerosol containing atmospheres, because the Rayleigh scattering cross-section decreases with wavelength ( $\lambda^{-4}$ )
- ~ The detection of aerosol properties with Lidar requires *a priori* assumptions and is limited to abundance, and size distribution. Almost no information about composition could be successfully retrieved yet. This limitation is particularly severe, since particles are present in the atmosphere as a broad distribution of size (from 10 nm to 100  $\mu$ m), shape (spherical, fractal, crystals, aggregates, etc.), and composition (water, soot, mineral, bioaerosols, *e.g.*, bacteria or viruses, etc.).

In 1998, a pioneering experiment demonstrated that most of the above mentioned difficulties might well be overcome by employing atmospheric white light plasma channels [34,35]. Intense ultra-short pulses from a high-power femtosecond laser (220 mJ 100 fs) were shined vertically into the sky and permitted to observe for the first time the phenomenon of white light generation in an extended plasma channel in the atmosphere. Time-resolved measurements of the backscattered white light using a Lidar set-up showed atmospheric propagation at altitudes as high as 12 km. This experiment opened a new field of Lidar investigations: The white light femtosecond Lidar technique based on the non-linear propagation of ultra-short and ultra intense laser pulses in the atmosphere.

Moreover, it was realized that white-light generation originated from a non-linear propagation regime specific to very high peak power laser pulses, called filamentation [3], in which a significant part of the beam energy self-guides into a thin light channel over lengths much longer than the Rayleigh length. Besides Lidar, such filaments open the way to

spectacular atmospheric applications, such as laser-assisted cloud condensation, or lightning control.

On the basis of those first experiments, a large-frame French-German project, "Teramobile" (for "Terawatt laser in a mobile system") was launched in 1999. The aim of the project was to construct the first mobile Terawatt-Laser based Lidar, *Teramobile*, in order to investigate fundamental processes like long-range propagation and filamentation, and new possibilities of probing the atmosphere. The Teramobile system has been the only mobile Terawatt laser for almost 8 years. Recently, the interest for atmospheric applications of ultrashort lasers gave rise to a couple of developments throughout the world, including the TNT (Terawatt and Terahertz) laser of DRDC Valcartier in Canada.

After recalling briefly the physics of filamentation, we review such applications in the following of the present paper.

## 2. Non-linear propagation of TW pulses

Developing applications of non-linear propagation of ultrashort pulses and filamentation requires understanding of the underlying physical mechanisms that govern this specific propagation regime. In the present section, we develop a qualitative discussion to focus our attention on the physical origin of the processes at play rather than their mathematical description. The reader is referred to more specific reviews about non-linear propagation of ultraintense laser pulses [36,37,38] for an analytical description of these processes.

### 2.1 Kerr self-focusing

At high powers, the refractive index of the air is modified by the Kerr effect [10,11]:  $n = n_0 + n_2 I$ , where  $I$  is the incident intensity. As the intensity in a cross-section of the laser beam is not uniform, the refractive index in the center of the beam is larger than on the edge (Fig. 1(a)). Since  $n_2$  in air is positive, this induces a radial refractive index gradient equivalent to a converging lens (called 'Kerr lens'). If the beam power exceeds a critical power  $P_{cr}$  of a few GW in air, Kerr effect overcomes diffraction and the beam is focused by this lens, which leads to intensity increase and shorter focal length lenses, until the whole beam collapses at a distance which depends on the initial beam power [45]. Kerr self-focusing should therefore prevent propagation of high power lasers in air if it was the only process at play.

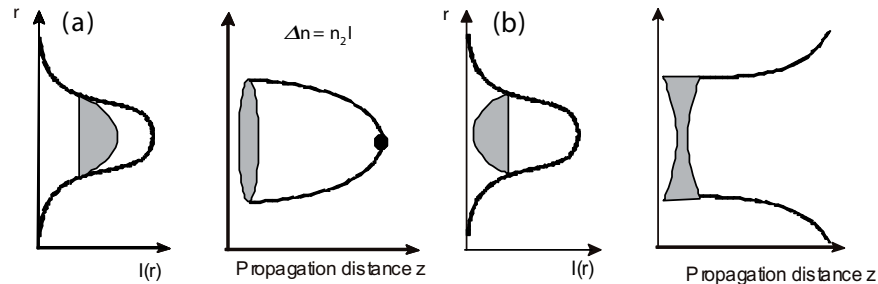


Fig. 1. Principle of filamentation. (a) Self-focus and collapse of the beam due to the Kerr effect. (b) Ionization at the non-linear focus then defocuses the beam. [39]

### 2.2 Multiphoton ionization and plasma generation

If the laser pulse intensity reaches  $10^{13}$ - $10^{14}$  W/cm<sup>2</sup>, higher order processes occur such as multiphoton ionization (MPI). At 800 nm, 8 to 10 photons are needed to ionize N<sub>2</sub> and O<sub>2</sub> and give rise to plasma [40]. The ionization process can involve tunneling as well, because of the very high electric field carried by the laser pulse. However, following Keldysh's theory [41], MPI dominates for intensities lower than  $10^{14}$  W/cm<sup>2</sup>. In contrast to longer pulses, fs pulses combine high ionization efficiency due to their very high intensity, with a limited overall energy, so that the generated electron densities ( $10^{16}$ - $10^{17}$  cm<sup>-3</sup>) are far from saturation. Losses

by inverse Bremsstrahlung are therefore negligible. Nevertheless, the electron density  $\rho$  induces a negative variation of the refractive index, and a negative refractive index gradient. This acts as a diverging lens, which defocuses the laser beam, as schematically shown in Fig. 1(b).

### 2.3 Filamentation of high power laser beams

Although Kerr self-focusing and plasma defocusing should individually prevent long distance propagation of high power laser beams, in combination they can come to a dynamic balance. In this regime, they exactly compensate and give rise to a self-guided quasi-solitonic [42] propagation. The laser beam is first self-focused by Kerr effect. This focusing then increases the beam intensity and generates plasma by MPI, which in turn defocuses the beam. The intensity then decreases and plasma generation stops, which allows Kerr re-focusing to take over again. This dynamic balance between Kerr effect and plasma generation leads to the formation of stable structures called "filaments" (Fig. 2). Light filaments were first observed by A. Braun *et al.* [3], who discovered that mirrors could be damaged by high-power ultrashort laser pulses even at large distance away from the laser source. These light filaments have remarkable properties. In particular, they can propagate over several hundreds of meters, although their diameter is only 100-200  $\mu\text{m}$ , thus widely beating the usual diffraction limits. Moreover, they keep an almost constant (or "clamped" [43]) intensity (typically  $10^{14}$   $\text{W}/\text{cm}^2$  [44]), energy (some mJ) and diameter.

Most of the numerical descriptions of filamentation rely on the non-linear Schrödinger equation (NLSE) [42], which is derived from Maxwell's wave equation in paraxial conditions, using the slowly-varying envelope approximation (SVEA) [45]. Numerically solving the NLSE equation leads to the evolution of the pulse intensity as a function of propagation distance. Initial Kerr lens self-focusing and subsequent stabilization by the MPI-generated plasma are well reproduced by these simulations.

For laser powers widely exceeding the critical power, the beam breaks up into a large number of localized filaments. The intensity in each filament is clamped at  $10^{13}$  -  $10^{14}$   $\text{W}/\text{cm}^2$  [43,44] corresponding to a few mJ, so that an increase in power leads to the formation of more filaments. Recent measurements reported that one filament is generated for each 5 critical powers, and this for the whole range of laser powers technically available [46,47]. Figure 2 shows a cross-section of laser beams undergoing mono-filamentation (Fig. 2, 5 mJ) and multifilamentation (Fig. 2, 400 mJ). The stability of these structures is remarkable: filaments have been observed to propagate over hundreds of meters [39,48] and can be initiated some kilometers away from the laser source [49,50].

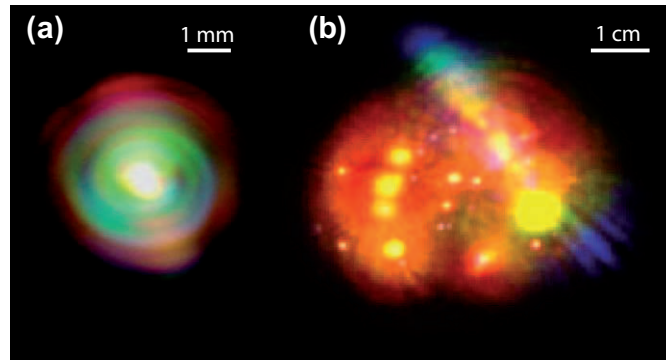


Fig. 2. (a) Conical emission observed on a screen; (b) Multifilament pattern on a screen [51].

Many theoretical studies have been carried out to simulate the non-linear propagation of high power laser beams, both in the mono-filamentation [45,53,54,55,56,57,58,59,60] and in the multi-filamentation [50,61,62,63,64,65,66] regimes. A comprehensive review of these simulations is, however, beyond the scope of this article.

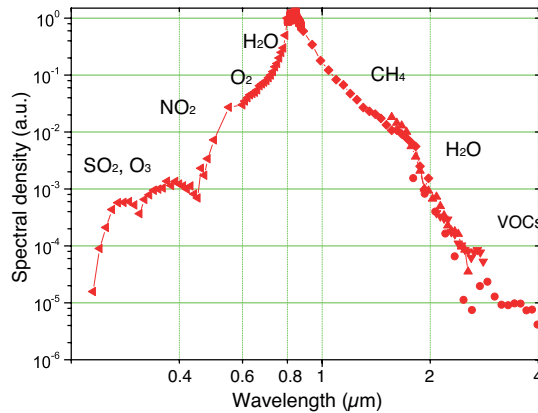


Fig. 3. Spectrum of the white light continuum. Absorption bands of some atmospheric species are indicated. [52]

At extreme power and energy levels (thousands times the critical power), the scalability of the results described above is not straightforward, and it is a particular challenge to understand laser propagation. The non-linear Schrödinger equation used to model propagation at TW levels [42] may be altered by higher order terms which would prevent the formation of filamentary structures. For instance, over the critical plasma density, inverse Bremsstrahlung would stop beam propagation. However, using the *Alisé* beamline (26 J, 32 TW pulses) of CEA-CESTA [67], the scalability of the filamentation regime was investigated for powers and energies larger by respectively one and two orders of magnitude compared to the previous ones. Extreme power laser pulses turned out to generate multiple (up to 400, proportional to the beam power) filaments through processes remarkably similar to those observed for sub-Joule pulses [47]. Although conversion into the supercontinuum is less efficient than with shorter pulses (a few percent), the supercontinuum propagates up to the stratosphere, beyond 20 km. This result constitutes the highest power “white-light laser” demonstrated to date. It suggests that further increasing energy may help developing atmospheric applications.

#### 2.4. White light generation and self-phase modulation (SPM)

The spectral content of the emitted light is of particular interest for applications, especially for Lidar. Non-linear propagation of high intensity laser pulses does not only provides self-guiding of the light and remote delivery of high intensities, but also an extraordinary broad continuum spanning from the UV to the IR. This supercontinuum is generated by self-phase modulation as the high intensity pulse propagates. As depicted above, Kerr effect leads, because of the spatial intensity gradient, to self-focusing of the laser beam. However, the intensity (and thus the refractive index) also varies in time, so that the most intense slice of the pulse, *i.e.* its center, is more retarded than its wings. Therefore, the electromagnetic wave on the rising edge is stretched, resulting in longer wavelengths, while the trailing edge is compressed and generates shorter wavelengths. This deformation of the carrier of the pulse results in a strong spectral broadening around the central wavelength. Figure 3 [68,69] displays the spectrum emitted by filaments that were created by the propagation of a TW laser pulse. The supercontinuum spans from 230 nm to more than 4 μm, which covers absorption bands of many trace gases in the atmosphere (methane, VOCs, CO<sub>2</sub>, NO<sub>x</sub>, H<sub>2</sub>O, etc.). UV generation is supported by third harmonic generation (THG) and frequency mixing [70,71]. Since the white-light continuum is generated through coherent  $\chi(3)$  processes, it retains the coherence of the incident laser beam, although the broad spectral range leads to a shorter coherence length. This coherence allows the continuum from neighboring filaments to interfere [72], and is the origin of the term “white-light laser” [73] which is sometimes used to depict the continuum.

### 2.5. Angular distribution of the supercontinuum emission

Most of the filamentation studies showed that white light is generated in the filamentary structure, and leaking in form of a narrow cone in the forward direction (called "conical emission," see Fig. 2(a)) due to coupling with the self-generated plasma [74,75]. This cone spans from the longer wavelengths in the center to the shorter wavelengths at the edge, with a typical half-angle of  $0.12^\circ$ .

An important aspect for Lidar applications is the angular distribution of the white light continuum in the near backward direction. The emission close to the backward direction of the supercontinuum from light filaments was found to be significantly enhanced as compared to linear Rayleigh-Mie scattering [76]. Figure 4 shows the comparison of the linearly backscattered light (Rayleigh-Mie) from a weak laser beam and the non-linear emission from a filament, for both *s*- and *p*-polarizations. At  $179^\circ$  the non-linear scattering exceeds the linear one by one order of magnitude. An even greater enhancement is expected at  $180^\circ$ . Combined with self guiding that drastically reduces beam divergence, this aspect is extremely important for Lidar experiments: most of the white light emitted from the distance *R* is then collected by the Lidar receiver, unlike conventional elastic scattering from white light sources, such as flashlamps based Lidars. [77].

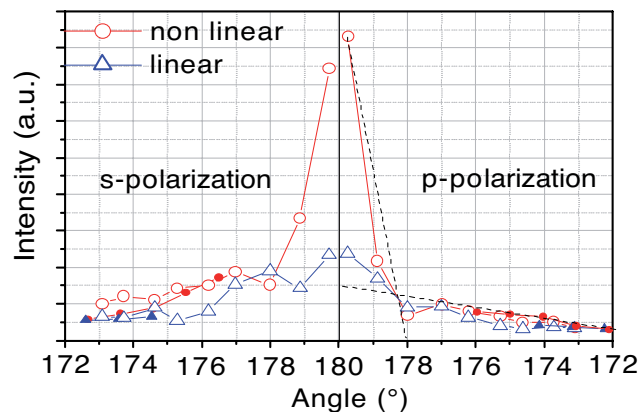


Fig. 4. Comparison of the linearly backscattered light (Rayleigh-Mie) from a weak laser beam and the non-linear emission from a filament, for both *s*- (left) and *p*- (right) polarizations

To summarize, non-linear propagation of TW-laser pulses provides unique properties for multispectral Lidar measurements: extremely broadband coherent light emission ("white light laser"), confined in a self-guided beam, and partially back-reflected to the emitter as the laser pulse propagates.

### 2.6. Propagation of laser filaments at high altitude

Since filamentation counteracts diffraction over long distances, it allows delivering high laser intensities at high altitudes. This contrasts with linear propagation, in which the laser intensity always decreases while propagating away from the source.

The distance at which high powers are reached and thus where filamentation starts, can be controlled by the following laser parameters: the initial laser diameter and divergence, the spatial profile and the pulse duration and chirp [78]. Temporal focusing consists in using an initial chirp together with the air GVD to obtain the shortest pulse duration (and thus the onset of filamentation) at the desired location. The compressor is aligned in such a way that a negatively chirped pulse is launched into the atmosphere, *i.e.* the blue component of the broad laser spectrum precedes its red component. In the near infrared, air is normally dispersive, and the red components of the laser spectrum propagate faster than the blue ones. Therefore, while propagating, the pulse shortens temporally and its intensity increases. At the preselected altitude, the pulse recovers its initial duration and non-linear effects like filamentation start.

(Fig. 5). As detailed in Section 2.9.1 below, the pressure gradient associated with altitude does not affect the filamentation dynamics significantly.

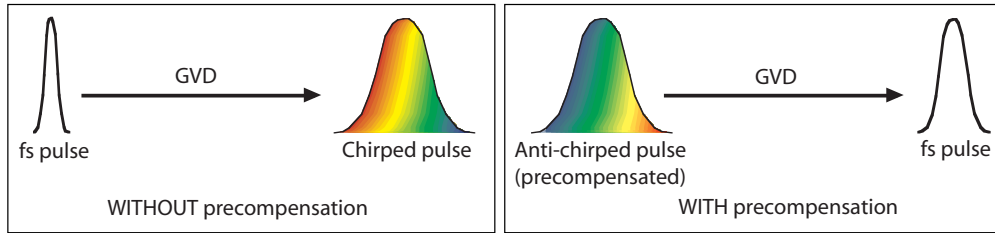


Fig. 5. Principle of temporal focusing. Left: an initially Fourier-limited pulse is chirped by group-velocity dispersion in the air. Right: an initially anti-chirped pulse is recompressed (temporally focused) by GVD during its propagation in the atmosphere.

Chirp-based control of supercontinuum generation has been demonstrated using the 2 m diameter telescope of the Thüringer Landessternwarte Tautenburg (Germany). For these experiments, the Teramobile laser was placed next to the astronomical telescope [49]. The laser beam was launched into the atmosphere and the backscattered light was imaged through the telescope. Figure 6(a) shows a typical image at the fundamental wavelength of the laser ( $\lambda = 800$  nm), over an altitude range from 3 to 20 km. In this picture, strong scattering is observed from an aerosol layer at an altitude of 9 km (and weaker around 4 km). As shown in Fig. 6(b), (c) and (d), the same observation can be performed in the blue-green band of the white-light continuum (385 to 485 nm). In aerosol-free conditions, white-light backscattered by Rayleigh scattering was detected up to 18 km. Filamentation and white light generation strongly depend on the initial chirp of the laser pulse, *i.e.* white-light signal can only be observed for adequate GVD precompensation (Fig. 6(b)).

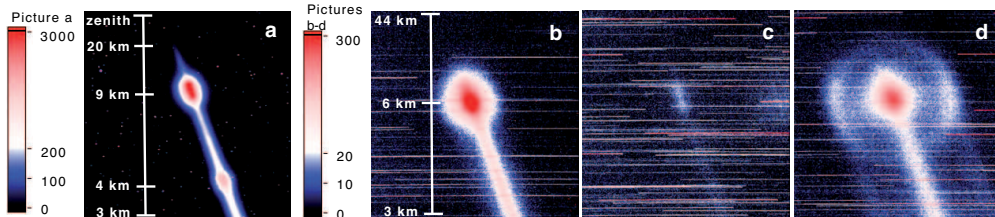


Fig. 6. Pictures of the *Teramobile* fs-laser beam propagating vertically, and imaged from the ground. (a) Fundamental wavelength. (b, c, d) White-light (385-485 nm) emitted by the femtosecond laser beam: (b) With GVD precompensation. (c) Without GVD precompensation. (d) With slight GVD precompensation. Notice the conical emission imaged on a haze layer. [95]

Conical emission was also imaged on the haze layer (Fig. 6(d)). Since conical emission is emitted sideways over the whole channel length, the visible rings indicate that under these experimental conditions (slight antichirping), the channel was restricted to a shorter length, and triangulation permits to determine its altitude. Conversely, this altitude was up to 2 km for adequate GVD precompensation [49].

### 2.7 Noise reduction through spectral correlations

Studies on optical fibers showed that spectral correlations and squeezing occur for temporal solitons [79,80,81,82,83,84,85,86]. The origin of correlations in the intensity fluctuations within the white light continuum is intrinsic to spectral broadening by  $\chi^{(3)}$  Kerr effect [87,88]. Such  $\chi^{(3)}$  broadening includes both self-phase modulation (SPM), cross-phase modulation (XPM) and four-wave mixing (FWM). SPM and XPM correspond to the deformation of the temporal envelope of the pulse, related to the carrier phase, while FWM describes the

interaction of two specific waves at wavelengths  $\lambda_0$  and  $\lambda'_0$ , which are converted into a pair of photons at the conjugated wavelengths  $\lambda_1$  and  $\lambda_2$ , for which the energy conservation imposes  $1/\lambda_0 + 1/\lambda'_0 = 1/\lambda_1 + 1/\lambda_2$ . Both SPM and FWM result in typical correlation maps within the spectrum at the exit of the fiber. The wavelengths within the side of the continuum appear anticorrelated with the central one, while pairs of conjugated wavelengths are strongly correlated [79]. Such correlation maps are very well reproduced by numerical simulations in optical fibers [89].

Since the white-light continuum in filaments also originates from  $\chi^{(3)}$ -processes, similar correlations can be expected, although the high intensity needed restrict correlations to the classical domain. Indeed, intensity correlations, as well as laser noise compression, have recently been reported for laser filaments in air [90,91], and of UV filaments in Argon [92]. Before filamentation, correlations are observed in the regions corresponding to  $\lambda_1 = \lambda_2$ . Once filamentation occurs (Fig. 7(b)), SPM is initiated, and positive correlations are observed in regions corresponding to nearly conjugated wavelengths ( $2\omega_0 = \omega_1 + \omega_2$ ). In contrast, negative correlations form a dark cross centered on the fundamental wavelength. In other words, fundamental wavelength is depleted to simultaneously generate both the Stokes and the anti-Stokes components of the continuum [90]. As is observed in fibers, further propagation of the filament (Fig. 7(c)) results in a more complicated structure of the correlation map. Stripes of positive and negative correlations appear around the fundamental wavelength because of the typical oscillatory structure of the supercontinuum generated by  $\chi^{(3)}$  broadening: Each wavelength is generated by two time slices of the pulse with the same temporal derivative of the intensity, resulting in interferences [93]. A similar build-up of correlations is observed when recording the correlation maps for increasing peak power at a given location, and for increasing pressure (*i.e.*, the non-linear refractive index) within an Argon cell. Indeed, following the empirical Marburger's formula [94], increasing either the propagation distance, the non-linear refractive index or the peak power both result in moving to later filamentation stages. After the filament ends, the correlation map does not evolve anymore since the laser intensity is too low to produce further  $\chi^{(3)}$ -induced broadening.

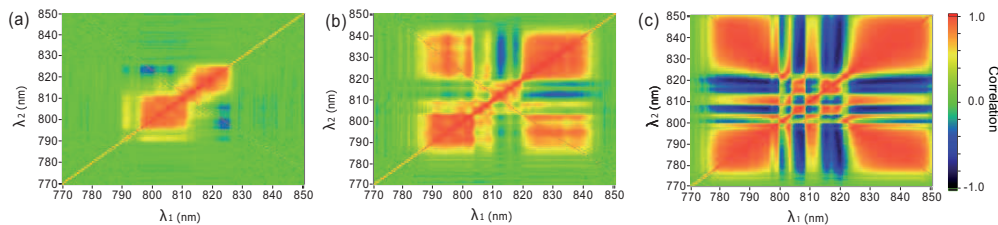


Fig. 7. Correlation maps within the white-light spectrum at the fixed peak power of 6.5 GW (~ twice the critical power for filamentation). (a) Before filamentation ( $z = 2$  m); (b) Filamentation onset ( $z = 3.5$  m); (c) Filament end ( $z = 8$  m) [91]

The correlation maps observed in filaments are very similar to those obtained from numerical simulations which do not take ionization nor other higher order processes into account, in both temporal solitons (*i.e.* in fibers) [89] and in air [91]. This confirms that plasma does not play a significant role in the build-up of the correlations.

The occurrence of correlations allows intensity noise reduction for adequately selected spectral regions. Applications such as high sensitivity multi-pollutant detection with a “white-light lidar” [95] or molecular coherent control with closed-loop schemes [96,97,98,99] would greatly benefit of a reduced shot-to-shot noise on the supercontinuum intensity. The noise reduction of the spectrally filtered supercontinuum is defined as  $-10\ln(V(I_{filament})/V(I_{ref}))$ , where  $V(x)$  denotes the variance of a parameter  $x$ , and  $I_{filament}$  and  $I_{ref}$  are the intensities associated with the filament and the unfocused laser beam taken as reference, respectively, integrated over the considered spectral interval. The optimal interval was determined to be

10 nm wide, centered on the fundamental wavelength. The noise reduction was up to 3.6 dB at the end of filamentation. This value is comparable to the squeezing achieved in fibers after correction for detection losses (*e.g.*, 4.1 dB in microstructured fibers [100] and 3.2 to 3.7 dB for classical fibers [101,102]). Noise reduction was even stronger for filamentation in Argon at 400 nm, reaching 7 dB. [92]

### 2.8 Control of filamentation

The possibility of controlling to a certain extent the basic features of non-linear propagation has been demonstrated using several strategies. The use of the initial focusing of the beam [103] has been proposed for a long time. More recently, effects induced by the initial pulse chirp (See 2.6) [39,49,50,104,105], spatial filtering [106], beam profile [107], pulse energy [46], initial focus [108], and polarization [109] have been investigated. Moreover, the advent of spatial light modulators (SLM) and acousto-optical modulators, which apply specific phase-shifts or modulating the intensity to each spectral component of the laser pulse, drastically increases the number of parameters that can be tuned to control filamentation, as was previously done for coherent control of atomic and molecular interactions [110,111,112].

However, both molecular optimal control and filament optimization are ill-posed problems, *i.e.* problems for which an explicit calculation of the solution is not possible, while the reverse problem can be solved or measured experimentally. In the case of filamentation, numerical simulations are time-consuming, so that the large number of available parameters prevents any *a priori* definition of the best laser conditions to optimize a specific property of the filaments. On the other hand, the target properties of the filaments (onset position, length, white-light bandwidth or intensity, plasma density...) are easy and fast to measure experimentally. Such problems can efficiently be addressed by closed-loop, non-deterministic algorithms such as genetic algorithms [113,114]. The optimization is performed by randomly generating a set of tentative solutions, test them by measuring the value of the experimental parameter to optimize, and generate a new set of tentative solutions by combining those yielding the best results. After some number of iterations, the population converges toward an optimal solution: The retrieved parameter set is often considered to bear information about the physical process at play [115]. Recently, several groups applied closed-loop optimizations to optimize diverse effects of filamentation.

Baumert *et al.* first demonstrated that a closed-loop optimization could be used to correct the chirp of an ultrashort laser pulse: By maximizing the yield of second-harmonic generation in a BBO crystal, they restored short pulses, compensating for the dispersion induced by propagation through a 150-mm long SF10 rod [96]. More recently, Heck *et al.* controlled the position of filaments in dye-doped water [97] by setting a region of interest on the filament picture recorded by a CCD. This target position as well as the filament length was given as the optimization goal to a genetic algorithm driving a SLM. This setup was able to move the filament location by more than 10 cm inside the cell. FROG measurements showed that the optimized pulses had a complex structure consisting of high order phase functions and multiple pulses in the time domain; Such shape could not have been obtained using a single parameter such as chirp or energy control.

In the spatial shaping domain, Walter *et al.* [98] used a 2-dimensional SLM driven by a genetic algorithm to control the spatial beam profile of a laser beam. Here, the goal was to avoid the formation of parasitic hot spots and concentrate the highest possible energy on a single filament. The optimization resulted in a more confined high-intensity region, and a slightly longer filament. Moreover, the spatial chirp of the beam was corrected efficiently, resulting in a more homogeneous spectrum across the beam profile.

The Teramobile team investigated the scalability of the above-described laboratory results to atmospheric problems [99]. Using a SLM and a genetic algorithm, we independently optimized three spectral regions within the white-light continuum, as well as the ionization efficiency, at ~30 m distance. Light from the supercontinuum was recorded in a Lidar configuration. The electron density was measured using sonometric measurements

[116,117,118]. The genetic algorithm was able to converge in spite of the fluctuations of both the laser system and the atmosphere where the laser propagated. It typically improved the signal by a factor of 2 for white light and 1.4 for ionization. The optimization yields a rich pulse shape that provides a stronger signal than could be obtained by adjusting the chirp alone. Contrary to what was observed at the laboratory scale [119], the same pattern optimizes all wavelength regions simultaneously. On the other hand, the optimization of the plasma yield at a given distance results in setting the filament onset at that distance, as could be expected from the fact that the plasma density is at its highest at the beginning of the filaments [116]. However, getting insights into the physics of filamentation from the pulse shape yielded by the closed-loop optimization is restricted by the high complexity of this shape. The fact that pulse shaping and closed-loop optimization works over long paths in the real atmosphere suggests that it could also be used to improve the selectivity of multiphoton-excited fluorescence Lidar for bioaerosol detection [120] or remote LIBS [121,122,123] in the future.

## 2.9 Filamentation in adverse conditions

Atmospheric applications of ultrashort laser pulses, such as free-space communication, Lidar remote sensing (See 3.1 and 3.2), telemetry, active imaging, lightning discharge control (see 3.4), or even tests of the general relativity effects in the earth gravitational field [124], require a comprehensive knowledge about the atmospheric propagation of ultrashort laser pulses in the atmosphere, under realistic conditions: Temperature or pressure gradients, turbulence, rain or fog. However, turbulence induces refractive index gradients that could be expected to jeopardize the dynamic balance between Kerr lens and plasma defocusing in the filaments. Aerosol particles, like water droplets or dust, can have dimensions of several tens of microns, comparable with the filament diameter: They could seriously harm the dynamical balance required to propagate filaments.

### 2.9.1 Filament interaction with aerosol particles and clouds

The first demonstration of the robustness of filaments was performed by launching it on a single droplet of 100  $\mu\text{m}$  diameter, produced by a piezoelectric nozzle synchronized with the laser [125]. Although the particle is expected to perturb the dynamical balance between Kerr self-focusing and defocusing by the plasma, the filament appears unperturbed by a droplet inserted downstream of its onset. Its length is not affected and its energy losses are very limited. Similar results were obtained with opaque particles. This survival of the filament after interacting with a droplet is due to the fact that the filaments contain only one third of the beam energy. The remaining propagates around it as a “photon bath” of typically 2 mm diameter. This “reservoir” [61] dynamically exchanges energy with the filament and provides the required energy for further propagation. [108,126,127,128].

This interpretation was confirmed by symmetrical observations showing that the filamentation is stopped by a diaphragm of about 300  $\mu\text{m}$  diameter, larger than the filament diameter but blocks the photon bath [129,130]. Recent simulations by Skupin *et al.* [131] confirmed that the region of the photon bath efficiently contributing to the filament feeding has a typical diameter of 350  $\mu\text{m}$ . Associated with the filament core of 100  $\mu\text{m}$  diameter, this bath constitutes a stable system. This description provides an interface between the dynamical instability model [53], in which the filament exchanges energy with the surrounding beam, and the description of filamentation in terms of quasi-solitons.

The transmission of filaments through a cloud depends on the transmission of the photon bath that can re-feed it after its interaction with obscurants. Indeed, a single filament appears unaffected after propagating through a synthetic cloud optically as thick as a cumulus or a stratocumulus [125]. Denoting  $P_T$  the transmitted power, the number of filaments observed is roughly equal to  $P_T/P_{cr}$ , independent on the presence of fog [46]. Filaments have even been initiated in natural rain conditions (150 m visibility), as well as at high altitude at reduced pressure (3,200 m altitude, *i.e.* 0.7 bar) [132].

As a summary, the filaments generated by ultrashort laser pulses can survive their interaction with a droplet of diameter as large as that of the filaments themselves. Moreover,

filaments can be transmitted through a dense fog over a distance comparable with the visibility within the cloud. This survival is related to the capacity of the filaments to regenerate after they have met an obscurant, from energy fed by the photon bath surrounding them.

### 2.9.2 Propagation through turbulence

Besides clouds, atmospheric turbulence is the main perturbation encountered by laser pulses propagating in the atmosphere. Atmospheric turbulence can be described by Kolmogorov's theory [133], in which the difference in refractive index between two points only depends on the distance between those points. This theory introduces the refractive index structure parameter  $C_n^2$ , which is commonly used to characterize the turbulence strength. Typical values for atmospheric turbulence are  $10^{-15} < C_n^2 < 10^{-13} \text{ m}^{-2/3}$  [133].  $C_n^2$  can be determined experimentally by measuring the pointing stability of a laser beam and using the relation  $C_n^2 = \sigma_\theta^2 \cdot \Phi^{1/3} / (2.91 \cdot L)$ , where  $\sigma_\theta$  is the standard deviation of the angle of arrival,  $\Phi$  is the beam diameter and  $L$  the length of the turbulent path [134].

Experiments in the infrared [135] and in the ultraviolet [136], as well as numerical simulations [135,137,138] under “moderate” turbulence ( $C_n^2 = 3 \times 10^{-13} \text{ m}^{-2/3}$ , corresponding to the upper limit for atmospheric values) have shown that the pointing statistics of the filaments transmitted through turbulence obey a Rayleigh-distribution law. Moreover, they can propagate through localized, strongly turbulent regions, up to five orders of magnitude above typical atmospheric conditions [139]. Their survival is governed by the quantity  $C_n^2 \times L$ , rather than by the structure parameter alone [140]. Scaling of laboratory experiments suggests that half of the filaments would survive after  $L \sim 4 \text{ km}$  in a typical turbulent atmosphere. Obviously, turbulence is not a limiting factor for filamentation in the atmosphere.

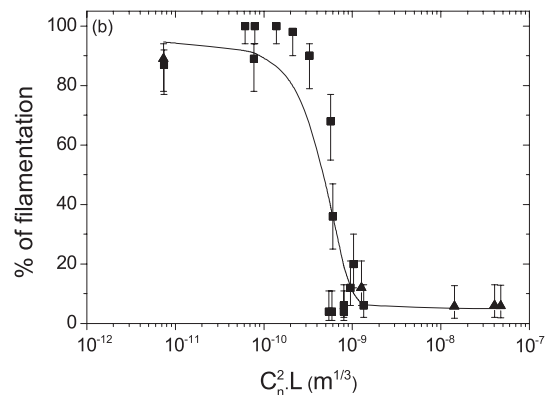


Fig. 8. Percentage of filaments surviving the turbulence as a function of  $C_n^2 \times L$ , ( $L$  being the turbulence length and  $C_n^2$  the structure parameter for the refractive index), in the case of localized (squares) and extended turbulent regions (triangles) located after the filament onset. [140]

Filaments that survived turbulence appear almost unaffected by the perturbation they have crossed. They have similar spectra than the ones transmitted through an unperturbed atmosphere. The shot-to-shot correlations between those spectra (See 2.7) are also maintained among filaments that have propagated across a turbulent region. Turbulence degrades the correlations only through the extinction of some of the filaments [140].

### 3. Atmospheric applications of laser filaments

#### 3.1. White-light Lidar measurements

##### 3.1.1. Gas-phase measurements

Ultra-intense laser pulses generate a broadband white-light source, which is ideal for Lidar applications. Since its backward-emitted component is significantly enhanced, it has a sufficient spectral density to allow spectroscopy for multicomponent analysis, contrary *e.g.* to arc-lamp-based Lidars [77]. This allows an efficient spectrally resolved Lidar (Fig. 9). Lidar signals have been measured in the UV-visible and the infrared parts of the continuum, from 230 nm [69] to 2.5  $\mu\text{m}$  [141], from altitudes of 2.5 km and 4.5 km, respectively.

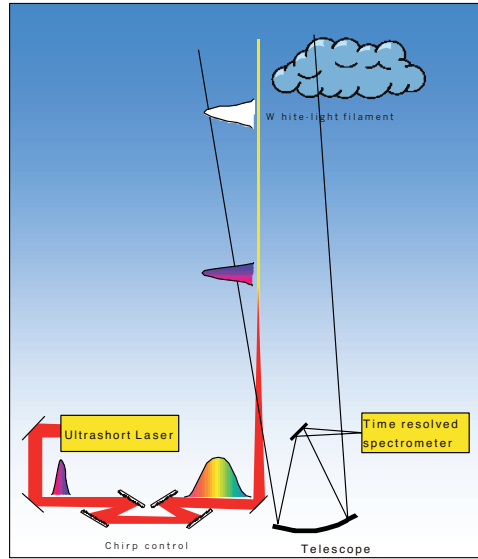


Fig. 9. Schematic of the fs-Lidar experimental setup. Before being launched into the atmosphere, the pulse is given a chirp to compensate for GVD during its propagation in air. Hence, the pulse recombines temporally at a predetermined altitude, where white-light continuum is produced, and then backscattered and detected by the Lidar receiver. [95]

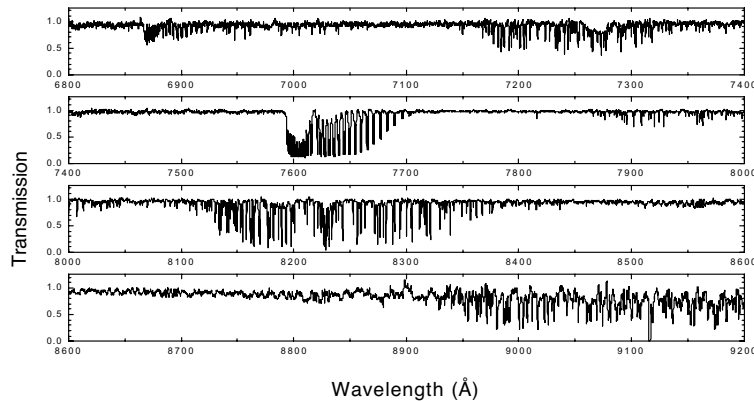


Fig. 10. High-resolution atmospheric absorption spectrum from an altitude of 4.5 km measured with the femtosecond white-light Lidar [95]

Figure 10 shows a spectrally resolved Lidar return from an altitude of 4.5 km, recorded with an intensified charge-coupled device (ICCD). The high resolution ( $0.1 \text{ cm}^{-1}$ ) spectrum

displays the well-known water vapor bands around 720 nm, 830 nm and 930 nm, simultaneously with the X  $\rightarrow$  A transition of molecular oxygen. This wide spectral range permits to use stronger or weaker H<sub>2</sub>O absorption bands, depending on the altitude (*i.e.* the water vapour concentration) in the spectrum analysis. Figure 11 shows fits of the water vapor (000)  $\rightarrow$  (211) transition and of the O<sub>2</sub> A band with the Hitran [142] database. It yields the water vapor mixing ratio as well as the temperature, and hence the *relative* humidity. These data are key parameters in understanding the physics of cloud formation and precipitation. The retrieved value is close to that measured by radiosonding, showing for the first time the ability of femtosecond white-light Lidar to perform simultaneous measurements of multiple atmospheric parameters [143]. This result was achieved with an instrumental resolution 10 times broader (0.1 Å) than would be required for the corresponding DIAL measurements of pressure or temperature profiles [144]. Such lower resolution was allowed by the use of the whole spectrum. The fit is performed over 700 data points, allowing for a deconvolution of the instrument function.

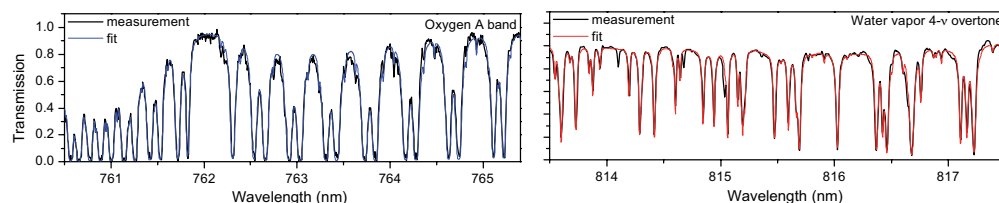


Fig. 11. Fit of (a) the O<sub>2</sub> A band in the 760-766 nm region and (b) the water vapor absorption spectrum in the 4v-overtone band at 813-816 nm. Black solid line: measurement; grey dotted line: fit [After Ref. 143]

### 3.1.2 Multispectral aerosol detection

The most advanced conventional Lidar methods for aerosol detection use several wavelengths (typically 2-5), usually provided by the fixed outputs of standard lasers (Nd:Yag, Ti:Sapphire, Excimers, CO<sub>2</sub>) [145,146,147]. The set of Lidar equations derived from the obtained multiwavelength Lidar data is subsequently inverted using sophisticated algorithms or multiparametric fits of pre-defined size distributions with some assumptions about the size range and complex refractive indices. In order to obtain *quantitative* mappings of aerosols, complementary local data (obtained with, *e.g.*, laser particle counters, or multi-stage impactors to identify the sizes and composition) are often used together with the Lidar measurements [22,148,149]. The determination of the size distribution and composition using standard methods must, however, be taken cautiously as complementary data, because of its local character in both time and space.

The white-light continuum provides a broadband light source with a continuous spectrum, particularly suitable for multispectral aerosol detection. Glavez *et al.* used the femtosecond supercontinuum generated in rare gas before transmitting into the atmosphere to perform multi-wavelength Lidar and characterize aerosols [150]. Since the continuum has the same polarization as the incident laser pulse, depolarization measurements are also possible. While the spectral analysis of such measurements is in principle an extension of the existing multi-wavelength algorithms, the presence of the filaments at a given altitude and the use of temporal focusing requires to update the Lidar equation and the inversion algorithms [78,151].

Multiple scattering of the white-light continuum is also a promising option. In addition to the relative humidity measurement described above, the white-light continuum was used to determine the size distribution and number density of water droplets within the cloud, by analyzing the white-light scattering from a cloud base. A cut across the scattering halo provided the angular pattern of multiple scattering, bearing information about the cloud droplet size and concentration. High-resolution images of the pattern around 800 nm provided for the first time a multi-field-of-view (multi-FOV [152,153,154,155]) Lidar at this angular resolution, which allowed to fit the size distribution in 18 size classes between 0.1 and 20 μm,

using a genetic algorithm. [113] Calculations were restricted to the scattering orders 1 (single scattering) through 3. The fitted size distribution was peaked around 5  $\mu\text{m}$ , in agreement with median values reported in the literature for continental stratus clouds. [156,157].

### 3.2 Non-linear Lidar

Ultrashort laser pulses are unique in that they remotely deliver very high intensities and have a short spatial and temporal extension. Both properties are the root of specific Lidar analysis techniques, especially for aerosol detection and analysis.

#### 3.2.1 Pump-probe measurements of droplet size through ballistic trajectories analysis

The very short extension of femtosecond pulses (50 fs are 11  $\mu\text{m}$  in water, i.e. the equator length of a 1.8  $\mu\text{m}$  sphere) open the way to direct geometrical analysis of aerosol particles. Stimulated processes such as stimulated Raman scattering (SRS) can only be observed in microdroplets when the spatial extension of the incident beam was larger than the droplet equator, allowing efficient feedback for stimulation [78]. This property was used to measure the size of microdroplets [158], and even to identify the ballistic trajectories used by the laser pulses within the microparticle. The latter experiment relied on a pump-probe experiment using two-photon excited fluorescence (2PEF) in dye-containing microdroplets. The droplets were used as optical correlators between two pulses circulating on ballistic orbits. Fluorescence was then recorded as a function of the time delay between the two pulses in order to quantify the path length traveled within the particle. 2PEF was only observed when the time delay between the two pulses was equal to an entire number of roundtrips. This experimental result was well reproduced by time resolved Lorentz-Mie calculations using plane wave excitation [159]. The simulations also showed that the effect would still be observable in particles as small as a few microns for 50 fs pulses, while shorter pulses could yield measurements of even smaller particles. In pump-probe 2PEF Lidar experiments, the composition would be addressed by the excitation/fluorescence signatures, and the size by the time delay between the 2 exciting pulses.

#### 3.2.2 Multi-photon excited fluorescence (MPEF) and ionization (MPI) in aerosol particles

Aerosol particles, and in particular spherical homogeneous microparticles (microdroplets) focus the incident beam onto small regions within themselves. Considering  $n$ -photon processes, the excitation map is proportional to the  $n$ -th power of the incident intensity, so that only molecules of the focus regions are significantly excited. The reciprocity principle ensures that the re-emission from these internal focal points is predominantly in the backward direction [160,161]: Re-emission from high-intensity regions tends to return toward the illuminating source by essentially retracing the direction of the incident beam that excited the particle.

This effect was demonstrated in the case of incoherent multiphoton processes involving  $n = 1$  to 5 photons, namely multiphoton-excited fluorescence (MPEF) of fluorophores- or amino acids-containing droplets ( $n = 1, 2, 3$ ) [160,161,162] and laser induced breakdown (LIB) in water microdroplets, initiated by multiphoton ionization ( $n = 5$  or more [163,164]). The backward enhancement, which is ideal for Lidar experiments, strongly increases with the order  $n$  of the multiphoton process. The anisotropy of the emission is characterized by the ratio  $R_f = U(180^\circ)/U(90^\circ)$  of the backward to side emissions. It increases from 1.8 to 9 for MPEF in Coumarin 510-doped ethanol droplets when  $n$  rises from 1 to 3, and exceeds 35 for LIB in aqueous droplets. Another remarkable property is that the backward enhancement is insensitive to the size if the droplet diameter exceeds some micrometers [165]. Moreover, both MPEF and LIB have the potential of providing information about the aerosol composition.

#### 3.2.3 Application to Bioaerosol Detection

Microdroplets containing biological fluorophors such as riboflavin are good models to demonstrate the advantage of combining MPEF and Lidar techniques to identify airborne

bacteria in the atmosphere [166,167]. This demonstration was performed in a cloud of typically  $10^4$  droplets/cm<sup>3</sup> with a typical size of 1  $\mu$ m, typical of airborne bacteria. Riboflavin was excited with two photons at 800 nm and emitted a broad fluorescence around 540 nm, at a distance of 45 m away from the excitation laser source, the Teramobile system. This experiment was the first demonstration of the remote detection of bioaerosols using a nonlinear femtosecond Lidar (Fig. 12 [120]). The broad fluorescence signature is clearly observed from the particle cloud, with a range resolution of half a meter, limited by the fluorescence lifetime of 3 ns for this transition [168]. As a comparison, droplets of pure water did not exhibit any parasitic fluorescence in this spectral range.

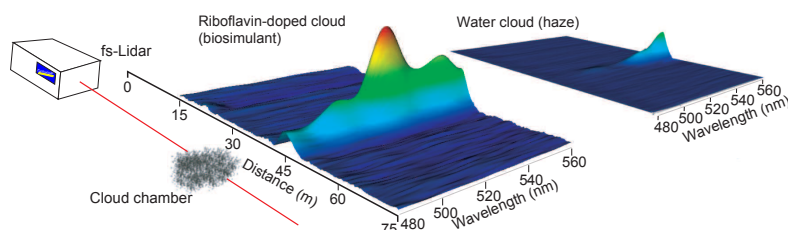


Fig. 12. Remote detection and identification of bioaerosols. The femtosecond laser illuminates a plume of riboflavin (RBF) containing microparticles 45 m away (left). The backward emitted 2-photon excited fluorescence (2PEF), recorded as a function of distance and wavelength, exhibits the specific RBF fluorescence signature for the bioaerosols (middle) but not for pure water droplets (simulating haze, right) [120]

MPEF might be advantageous as compared to linear laser-induced fluorescence (LIF) for the following reasons: (1) MPEF is enhanced in the backward direction and (2) atmospheric transmission is much higher for longer wavelengths. For example, if we consider the detection of tryptophan (another typical biological tracer that can be excited with 3 photons of 810 nm), the transmission of a clear atmosphere is typically 200 times higher at 810 nm than at 270 nm, although the exact factor depends on the background ozone concentration [169]. Simulations show that beyond a few kilometers, the non-linear fluorescence signal would be stronger than its linear counterpart. At this distance, the Lidar return of  $\sim 1$  photon/pulse still permits Lidar detection. The most attractive feature is however the possibility of using pump-probe techniques, as described above, to measure both composition and size through the length of ballistic trajectories.

### 3.2.4 “Clean fluorescence”

The high intensity delivered by the filaments could also be applied for remote sensing of gaseous pollutants by generating a breakdown in the air and analyzing the fluorescence spectrum of the excited species. Iwasaki *et al.* demonstrated that, due to their low energy for a given peak power, the obtained fluorescence spectra are free from the usual blackbody background: This “clean fluorescence” [170] could be used to characterize gaseous fluorophors in the atmosphere. This idea has already been demonstrated on the laboratory scale in the case of nitrogen [171] halocarbons, namely the PFCs CF<sub>4</sub> and C<sub>2</sub>F<sub>6</sub>, and HCFC-124 (2-chloro-1,1,1,2-tetrafluoroethane) [172]. The results most approaching real-conditions measurements were obtained on ethanol vapor, with a concentration of 0.8%: The corresponding fluorescence was measured at 10 m distance in a Lidar configuration [173]. However, extrapolation of these results to the kilometer-scale is not straightforward because the excitation and the collection efficiencies decrease together for increasing distances.

### 3.5 Raman-, CARS- and LIBS-based remote sensing techniques

Significant progress has been recently achieved for detecting bioaerosols using Raman spectroscopy with femtosecond lasers [174,175,176]. Particular interest has been dedicated to

bacteria and spores, for which calcium dipicolinate is a specific tracer [177]. Single bioparticles could be identified using Micro-Raman and advanced data classification techniques. Coherent Anti-Stokes Raman Scattering (CARS) is much more sensitive than spontaneous Raman, and is therefore widely preferred for practical applications that address small ensembles of bioparticles. A major drawback of the CARS detection of bacteria in air or in solution is, however, parasitic non-resonant four wave mixing (FWM) occurring in the matrix or in other species than the target molecules. This parasitic background often covers the vibrational signatures of the molecules of interest. Another limitation is fluorescence of the target molecules, in case of resonant Raman scattering. The combination of coherent control schemes and Raman spectroscopy recently opened exciting perspectives to overcome these problems [178,179,180,181]. They rely on the preparation of a coherent superposition of vibrational levels in the ground state using stimulated Raman scattering. Then, this superposition of levels is used in a CARS scheme. In particular, the group of M. O. Scully recently reported promising CARS methods, referred to as FAST-CARS [176] and hybrid CARS [175] in order to extract the Raman lines of bacterial spores from the background noise.

The use of femtosecond Raman schemes for the remote detection and identification of aerosols in the atmosphere was originally proposed by Kasparian *et al.* [78]. The method is based on a pump-probe SRS technique involving the ballistic propagation of femtosecond pulses within the particles (*e.g.* water droplets) in order to remotely determine both the size and the composition of aerosols. They also introduced a first Non Linear Lidar Equation (NLLE), which is an extension of the well-known Lidar equation [21,22,169] that includes non-linear processes. More recently, M.O. Scully suggested to apply the FAST CARS method to identify bioaerosol clouds remotely using a Lidar arrangement as well [175].

Parallel to Raman Spectroscopy, Laser Induced Breakdown Spectroscopy (LIBS) provides interesting results for the identification of bacteria and spores. The use of femtosecond pulses provides two major advantages: low plasma temperature (reducing the blackbody background and parasitic lines from the air) and molecular signatures additional to the atomic ones. In particular native C-N molecular lines could be observed from bacteria [182,183]. Systematic studies also allowed analyzing five different species of bacteria. Line emissions from Na, Mg, P, K, Ca, and Fe have been measured to create a profile representative of each bacteria species. Quantitative differentiation and sorting could be made by placing bacteria in a six-dimension hyperspace with each of its axis representing a detected trace element [184].

High power ultrashort laser pulses also provide a decisive advantage for performing remote identification of aerosols in the air using LIBS: filamentation. Focusing a laser beam using linear optics is limited to short distances (some tens of meters) because of diffraction [185,186]. Filamentation overcomes this limitation as it provides the equivalent of an "extended focus" over hundreds of meters or more. The first demonstration of Remote Filament Induced Breakdown Spectroscopy (R-FIBS) has been performed on solid metal target about 100 m away from the laser. The resulting plasma lines were detected and identified using a spectrometer and a gated CCD in a Lidar arrangement [121,187,188]. Similar experiments have been performed since then by the group of S.L. Chin at Laval University, especially on solid (pellets) [189,190,191,192] and aqueous [193] biological samples.

Although femtosecond laser based remote identification of atmospheric aerosols relying on RAMAN/CARS or LIBS was not reported yet, these techniques are very attractive. As white-light differential absorption Lidar, they have the potential of providing the remote analysis of a target air volume and thus of detecting a large number of species simultaneously. The backward enhancement of the plasma light emission in femtosecond LIBS experiments on individual aerosol particles (see 3.2.2) is encouraging toward this goal.

#### 4. Future prospects

While the applications of filaments described above draw a rich panel of various uses, other fields opened by this particular propagation regime have not been fully opened yet. In this section, we review few of these emerging applications, which might be of high interest in the future.

##### 4.1 Pump-probe spectroscopy to distinguish bioaerosols from background organic particles in air.

Fluorescence Lidar might suffer of a high frequency of false identification because aromatics and polycyclic aromatic hydrocarbons (PAH) from organic particles and Diesel soot strongly interfere with biological fluorophors such as amino acids [168,194]. To overcome this limitation, a novel femtosecond pump-probe depletion (PPD) concept was recently developed [195]. It is based on the time-resolved observation of the competition between excited state absorption (ESA) into a higher lying excited state and fluorescence into the ground state (Fig. 13(a)) [196,197]. By varying the temporal delay between the pump and probe pulses, the dynamics of the internal energy redistribution within the intermediate excited potential surface  $S_1$  is explored. In principle, as different species have distinct  $S_1$  surfaces, discrimination capabilities can be enhanced in this fashion.

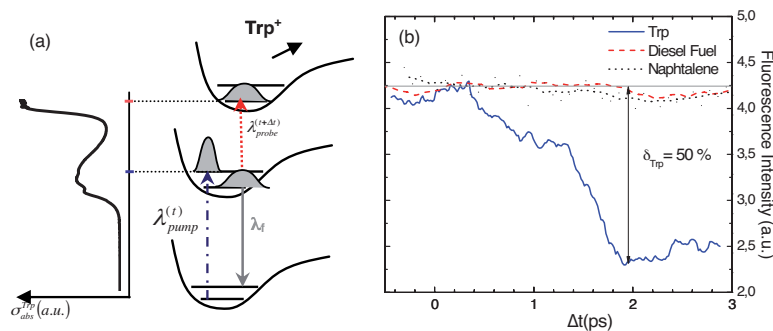


Fig. 13. Femtosecond pump-probe depletion (PPD) technique to distinguish biomolecules from organic intererents (a) Spectroscopic principle of the PPD [195]; (b) PPD applied to the distinction of Trp from traffic related PAH's

Figure 13(b) shows the pump-probe depletion dynamics of the  $S_1$  state in Tryptophan (Trp) in water, as compared to Diesel fuel and Naphtalene in cyclohexane, one of the most abundant fluorescing PAHs in Diesel. While depletion reaches as much as 50 % in Trp for an optimum delay of  $\Delta t = 2$  ps, Diesel fuel and Naphtalene appear almost unaffected (within a few percent), at least on these timescales. This remarkable difference allows for efficient discrimination between Trp and organic species, although they exhibit very similar linear excitation/fluorescence spectra. Two reasons might be invoked to understand this difference: (1) the intermediate state dynamics is predominantly influenced by the NH- and CO- groups of the amino acid backbone and (2) the ionization potential is higher for polycyclic aromatic hydrocarbons (PAH), so that excitation induced by the probe laser is much less likely in the organic compounds.

Similar results have been obtained with bacteria, including *Escherichia coli*, *Enterococcus* and *Bacillus subtilis*, which could be distinguished from Diesel fuel. These unique features can be used for a novel selective bioaerosol detection technique that avoids interference from background traffic-related organic particles in the air: The excitation shall consist of a pump-probe sequence and the fluorescence emitted by the mixture will be measured as the probe laser is alternately switched on and off. This pump-probe two-photon differential fluorescence method will be especially attractive for an active remote detection technique such as MPEF-Lidar (see 2.2.4), where the lack of discrimination between bioaerosols and transportation related organics is currently most acute. This technique can

even be extended with more sophisticated excitation schemes (*e.g.*, optimally shaped pulses), related to coherent control. It will not only improve discrimination between bioaerosols and non-bioaerosols, but also gain selectivity among the bacteria themselves. Recent theoretical calculations show that under some conditions, optimal dynamic discrimination (ODD) can lead to efficient distinction between three species that exhibit almost the same spectral characteristics [198].

#### 4.2 Phase transfer through the atmosphere

Coherent control techniques, especially when shaping is implied, require the spectral and spatial phase of the beam to be transmitted unaffected through the atmosphere up to the target. Transferring unaltered spectral phase through the atmosphere is also required for fast CARS (see 3.5). However, the local refractive index fluctuations associated with turbulence result in distortions of the wavefront and spectral phase of the pulse. Since the dephasings implied in pulse shaping are generally on the order of a fraction of  $\pi$ , this effect may be very critical, so that the transmission of shaped pulses could be expected to withstand much less turbulence than filaments do.

This question was investigated both experimentally, analyzing the beam profile, spectrum and autocorrelation trace of the transmitted pulses, and theoretically [199]. In strong turbulence, the beam profile exhibits a typical speckle pattern. In its low intensity regions, the pulse spectrum is depleted, and the pulse duration is increased. In contrast, the spectrum remains unchanged in the high intensity regions.

#### 4.3. Laser-triggered high-voltage discharges and lightning control

Filaments generated by ultrashort laser pulses may give rise to a spectacular application: The control of lightning strikes. Investigation on the physics of thunderbolts requires on-demand lightning strikes at a predetermined location. A technique to trigger lightning using rocket-pulled wires was developed in the 1970's [200,201]. But the number of rockets available for a given storm is limited. Therefore, the idea emerged to apply lasers to control lightning by ionizing the air along the beam, and forming a conducting plasma "wire." The first attempts, in the 1970's and 1980's, used nanosecond pulses [202,203,204]. They were unsuccessful, because such lasers cannot produce continuously ionized plasma channels because of the laser absorption by inverse Bremsstrahlung in the plasma generated at the leading front of the pulse. In contrast, promising results have been obtained using focused ultrashort laser pulses to trigger and guide high-voltage discharges over several meters in the laboratory [205,206]. Similar results have been obtained on smaller scales using UV ultrashort lasers [136].

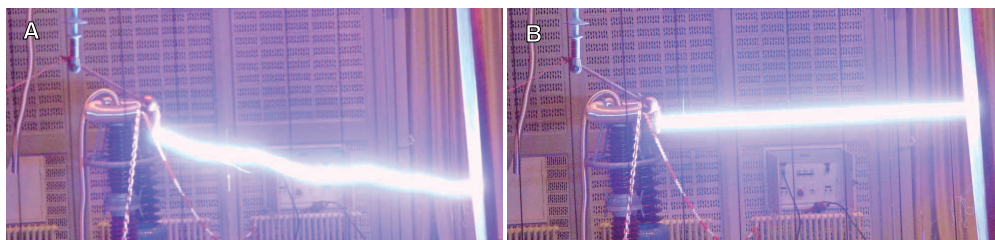


Fig. 14. Laser control of high-voltage discharges. (A) Free discharge over 3 m, without laser filaments. Note the erratic path. (B) Straight discharge guided along laser filaments. [95]

Filaments provide an even longer conducting path. They are particularly suitable for scaling such results to the atmospheric scales. Spectacular experiments with the Teramobile laser [39] installed in a high-voltage facility showed that laser filaments can trigger and guide 1.8 MV discharges over up to 4.5 m. The breakdown voltage is typically reduced by 30 % [207]. Moreover, triggered discharges are guided along the laser beam (Fig. 14). Partly guided discharges also occur in some configurations, providing information about the mechanism of the initiation and propagation of laser-triggered discharges [208]. Even artificial rain does not

prevent the laser filaments to trigger the discharges [209]. Current work focuses on the possibility to extend the plasma lifetime using auxiliary lasers in order to increase the possible guiding length and improve the scalability to atmospheric scales. This approach relies on re-heating and photodetaching electrons of the plasma channel by subsequent pulses, either in the nanosecond [136] or in the femtosecond regime [210]. Although a high power of the subsequent laser pulse is generally considered necessary for efficiently photodetaching electrons from  $O_2^-$  ions in the plasma, it was recently demonstrated that a subsequent YAG laser pulse of moderate energy (sub-Joule) at 532 nm efficiently increases of an infrared femtosecond laser [211]. This effect was interpreted as resulting from a positive retroaction loop where heating of the plasma channel by Joule heating enhances photodetachment, while the resulting higher electron density boosts the Joule effect. Therefore, the recent progresses in both laser science and high-voltage control experiments have brought this 30 years old dream much closer to reality.

#### 4.4 THz radiation emission and guiding

Laser filaments have been observed to emit electromagnetic radiation in remote bands such as the sub-THz region. Both transverse [212,213] and very directional forward and backward [214,215] emissions have been observed using heterodyne detection at 94 and 118 GHz as well as calorimetric measurements. The THz emission is efficient along the whole filament length, and is highly coherent, as demonstrated by interference experiments between emission from neighboring filaments, as well as between radial emission from the same filament section in opposite directions [216].

The THz emission was first interpreted as originating from the oscillation of the electrons in the plasma channel, due to a longitudinal charge separation induced by the radiation pressure of the laser pulse [217]. However, the polarization of the THz signal is independent of the laser polarization, instead of being parallel to the driving electric field of the incident laser. Therefore, Houard *et al.* [214] attribute the THz emission to a motion of the ionization front (*i.e.*, the creation of a dipolar charge distribution) faster than the speed of light in the medium [218], resulting in a Cerenkov emission.

Since THz emission is linked with the ionization front, it provides a non-contact technique to detect air ionization, besides sonometry [116,118], nitrogen fluorescence [219] and local conductivity measurements [16,220]. Moreover, the generation of a remote, directional THz source is favorable to remote THz imaging or absorption spectroscopy. While the transmission of such radiation in the air is poor, a local source avoids the losses associated with the propagation of the radiation towards the target, providing more efficient one-way absorption measurements.

Filaments may also be used to guide THz radiation [221]. Since the plasma frequency in typical filaments is in the sub-THz to THz range, they are opaque to such radiation, so that a filament grid could provide a THz reflector, while a circular array of filaments could lead to a THz waveguide so as to deliver THz radiation at remote predetermined locations.

## 5. Conclusion

The non-linear propagation of ultrashort ultra-intense laser pulses provides unique features for atmospheric applications, especially Lidar. A coherent supercontinuum, self-guided, is back-reflected towards the source. Backward enhancement also occurs for MPEF and LIB processes in aerosol particles. These characteristics open new perspectives for Lidar measurements in the atmosphere, such as multi-component detection, reduced spectral interference, better precision using more absorption lines, improved IR-Lidar measurements in aerosol-free atmospheres, and remote measurement of aerosols size distribution and composition. The ionized plasma channel left by the filaments is also very suitable to initiate condensation in supersaturated atmospheres, for which the ions provide condensation nuclei, as well as to control high voltage discharges, in a small-scale model for a laser lightning rod.

Here, the conducting plasma channel offers a preferential path for the discharge, allowing guided discharges to occur at a reduced breakdown voltage.

A wide spread of these techniques needs further characterization of the propagation of the laser pulses, in order to foresee the onset and the length of the filaments, and to better control the intensity at each location along the laser path. However, the convergent observations showing that filamentation is a robust feature that survives perturbed atmospheres constitute a significant path toward daily use.

The above-described applications will probably be also pushed forward in the future by improvements coming in the technology of ultrashort laser pulses: more reliable and compact systems, diode pumping, as well as spatial and temporal pulse shaping. New active media, such as Ytterbium doping [222,223] fiber lasers or OPCPA [224,225] open the way to compactness and new spectral regions, especially the infrared, which is nearer to the absorption region of many pollutants, such as VOCs, and where the eye-safety issues are easier to address. These more flexible systems should be easier to operate, opening the way to more routine use for implementing the applications currently under development, beyond the feasibility demonstration up to the precision and reliability of actual atmospheric measurements, for the routine production of relevant data.

### **Acknowledgments**

The authors acknowledge funding, especially in the framework of the Teramobile project ([www.teramobile.org](http://www.teramobile.org)), from the Centre National de la Recherche Scientifique (CNRS), the Deutsche Forschungsgemeinschaft (DFG), Agence Nationale de la Recherche (ANR, grant # NT05-1\_43175), Fonds national suisse de la recherche scientifique (FNS, grants #200021-111688/1 and 200021-116198/1), the Swiss Secrétariat d'État à l'Éducation et à la Recherche in the framework of the COST P18 project "The physics of Lightning Flash and its Effects,"

We gratefully acknowledge very fruitful discussion and common work with all the members of the Teramobile consortium, formed by the groups of L. Wöste in Berlin, J.-P. Wolf in Lyon and Geneva, R. Sauerbrey at the University Jena and A. Mysyrowicz at the ENSTA (Palaiseau), with a special mention of the technical staffs in Berlin, Jena, Geneva and Lyon. We would also want to mention fruitful collaboration with the group of L. Bergé at CEA/DPTA.